Journal of South American Earth Sciences 24 (2007) 203–227

Journal of
South American
Earth Sciences

www.elsevier.com/locate/jsames

Structural framework and Mesozoic–Cenozoic evolution of Ponta Grossa Arch, Paraná Basin, southern Brazil

Michael Strugale [a,1,2], Sidnei Pires Rostirolla [b,*], Fernando Mancini [b], Carlos Vieira Portela Filho [c], Francisco José Fonseca Ferreira [d,3], Rafael Corrêa de Freitas [e]

[a] Petróleo Brasileiro S.A. [PETROBRAS], Avenida Antônio Carlos Magalhães, 1113, sala 431, CEP 41.856-900, Salvador, Bahia, Brazil
[b] Universidade Federal do Paraná, Laboratório de Análise de Bacias e Petrofísica, Departamento de Geologia, P.O. Box 19027, 81.531-990 Curitiba, Paraná, Brazil
[c] Petróleo Brasileiro S.A. [PETROBRAS], Avenida Antônio Carlos Magalhães, 1113, sala 201, CEP 41.856-900, Salvador, Bahia, Brazil
[d] Universidade Federal do Paraná, Laboratório Pesquisa em Geofísica Aplicada (LPGA), Departamento de Geologia, P.O. Box 19001, 81.531-990 Curitiba, Paraná, Brazil
[e] Universidade Federal do Paraná, Laboratório de Análise de Bacias e Petrofísica, Departamento de Geologia, P.O. Box 19001, 81.531-990 Curitiba, Paraná, Brazil

Received 1 September 2003; accepted 1 November 2006

Abstract

The integration of structural analyses of outcrops, aerial photographs, satellite images, aeromagnetometric data, and digital terrain models can establish the structural framework and paleostress trends related to the evolution of Ponta Grossa Arch, one of the most important structures of the Paraná Basin in southern Brazil. In the study area, the central-northern region of Paraná State, Brazil, the arch crosses outcropping areas of the Pirambóia, Botucatu, and Serra Geral Formations (São Bento Group, Mesozoic). The Pirambóia and Botucatu Formations are composed of quartz sandstones and subordinated siltstones. The Serra Geral Formation comprises tholeiitic basalt lava flows and associated intrusive rocks. Descriptive and kinematic structural analyses reveal the imprint of two brittle deformation phases: D1, controlled by the activation of an extensional system of regional faults that represent a progressive deformation that generated discontinuous brittle structures and dike swarm emplacement along a NW–SE trend, and D2, which was controlled by a strike-slip (transtensional) deformation system, probably of Late Cretaceous–Tertiary age, responsible for important fault reactivation along dykes and deformation bands in sandstones.

Keywords: Paraná intracratonic basin; Ponta Grossa Arch; Mesozoic; Structural analysis; Aeromagnetometry; Lineaments

Résumo

A integração de dados estruturais de campo, aerofotografias, imagens de satélite, dados aeromagnetométricos e modelagem digital de terreno foi usada para determinar estilos estruturais e paleotensões relacionadas à evolução do Arco de Ponta Grossa durante o Cretáceo na Bacia do Paraná. O arco situa-se na região Sul do Brasil e apresenta expressivo enxame de diques acompanhando sua zona de

* Corresponding author. Fax: +55 41 3361 3642.
E-mail addresses: michael_strugale@petrobras.com.br (M. Strugale), rostirolla@ufpr.br (S.P. Rostirolla), ferman@ufpr.br (F. Mancini), cportela@petrobras.com.br (C.V. Portela Filho), francisco.ferreira@ufpr.br (Francisco José Fonseca Ferreira), rcdfreitas@ufpr.br (R.C. de Freitas).
[1] Present address: Petróleo Brasileiro S.A. [PETROBRAS] E&P/UN-BA/ATP-S/RES Av. Antonio Carlos Magalhães, 1113, sala 407, 41.856-900, Salvador, Bahia, Brazil. Fax: +55 71 3350 3789.
[2] Fax: +55 71 3350 3031.
[3] Fax: +55 41 3361 3642.

0895-9811/$ - see front matter © 2007 Elsevier Ltd. All rights reserved.
doi:10.1016/j.jsames.2007.05.003

charneira, constituindo a mais importante feição estrutural da borda leste da bacia. As unidades litoestratigráficas enfatizadas foram as formações Pirambóia, Botucatu e Serra Geral (Grupo São Bento, Mesozóico), as duas primeiras compostas por quartzo-arenitos e a segunda por derrames de basaltos toleíticos e corpos intrusivos associados. A análise estrutural indicou registros de dois eventos deformacionais rúpteis, D1 e D2, os quais relacionam-se a regimes tectônicos extensional e transtensional, respectivamente. O primeiro iniciou por controlar a intrusão do enxame de diques eo-cretáceos do Arco de Ponta Grossa e a partir daí desenvolveu deformação progressiva com a geração de falhas rúpteis descontínuas. O segundo, de provável idade neo-cretácea a terciária, promoveu importantes reativações nas paredes dos diques e a formação de bandas de deformação nos arenitos.

Palavras-chave: Bacia Intracratônica do Paraná; Arco de Ponta Grossa; Mesozóico; análise estrutural; aeromagnetometria; lineamentos

1. Introduction

This study provides a structural interpretation of mega-faults and tilting blocks along the axis of Ponta Grossa Arch and its associated dyke swarms, where it affects the permeable sandstones of the Pirambóia and Botucatu Formations in the central-northern state of Paraná, south Brazil (Fig. 1). The research is based on the identification of large, fault-delimited, morphotectonic compartments at kilometer and 10-kilometer scales. Descriptive, kinematic, and dynamic structural analyses of faults and joints observed in outcrops inside these compartments reveal the timing of tectonic events that affected the Pirambóia and Botucatu Formations. Another research goal is to evaluate Cenozoic tectonics and the associated descriptive aspects, kinematics, paleostresses, and fault reactivation events. Finally, a secondary research target is to understand the relationships among tectonic evolution, Early Cretaceous magmatism, and thermal uplift controlled by the opening of the South Atlantic Ocean.

The Paraná Basin is a vast sedimentary region in central South America whose deposition ranged from the Paleo-

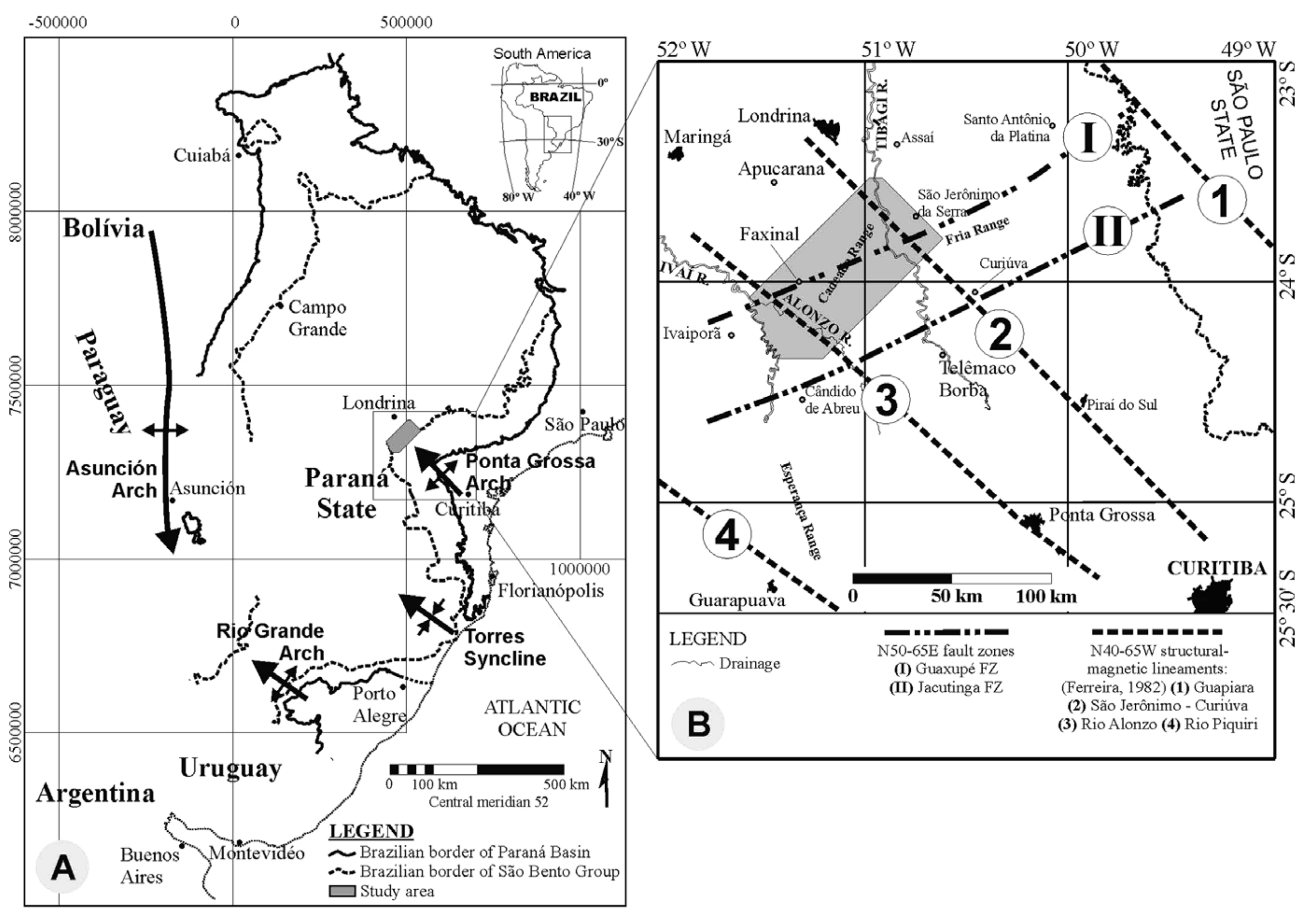

Fig. 1. (A) Regional geologic context of the study area showing main arched features in the eastern Paraná Basin border. (B) Study area location and structural-magnetic framework of central north Paraná (modified from Ferreira, 1982a,b; Zalán et al., 1990).

zoic to the Mesozoic. The basin is mainly composed of Late Ordovician–Late Cretaceous (Milani and Ramos, 1998) terrigenous rocks, with subordinate carbonates and igneous rocks, reaching up to 6000 m thickness. The long evolution of the Paraná Basin involves successive phases of subsidence and accumulation of massive depositional sequences limited by regional unconformities, which indicates important uplift and erosional events also occurred (Soares et al., 1978). These epeirogenic activities may reflect stress propagation from the nearest plate margin, related to convergent tectonics, intercalated with thermal effects and local extension in the plate interior. In this context, the Mesozoic opening of the South Atlantic Ocean represents an episode that triggered reactivation of basement faults and regional warping.

Ponta Grossa Arch is one of the most prominent structures in Paraná Basin (Northfleet et al., 1969; Vieira, 1973; Ferreira, 1982a,b). It strikes N45W, with faults extending for up to 10 km and throws reaching as much as 100 m, many of them filled with dolerite dykes. Fault systems present "en relay geometry," formed by planar or curvilinear individual faults. Four large N40–50W mega-fault zones (Vieira, 1973) define the structural framework of the arch and correspond to structural-magnetic features, named Guapiara, Rio Piquiri, São Jerônimo-Curiúva, and Rio Alonzo (Ferreira, 1982a,b) (Fig. 1). The Ponta Grossa Arch is responsible for important structural tilting and segmentation of Pirambóia and Botucatu layers. Aeromagnetometric data indicate that the dyke swarm extends for at least 300 km under the basaltic cover toward the depocenter of the Paraná Basin.

Stratigraphic units studied herein include siltstones and sandstones of the Rio do Rasto Formation (Passa Dois Group, Upper Permian), quartz sandstones of the Pirambóia (Triassic) and Botucatu (Jurassic–Cretaceous) formations, and mostly basic igneous rocks of the Serra Geral Formation (Cretaceous), São Bento Group (*sensu* Soares, 1975). Mafic dykes and sills emplaced in all units are also present in close temporal and genetic relation to basaltic flows of the Serra Geral Formation. The distribution and strong structural compartmentation of these units in the study area are shown in Fig. 2.

Descriptive structural analysis at different scales, including outcrop, aerial photographs, and Landsat TM7

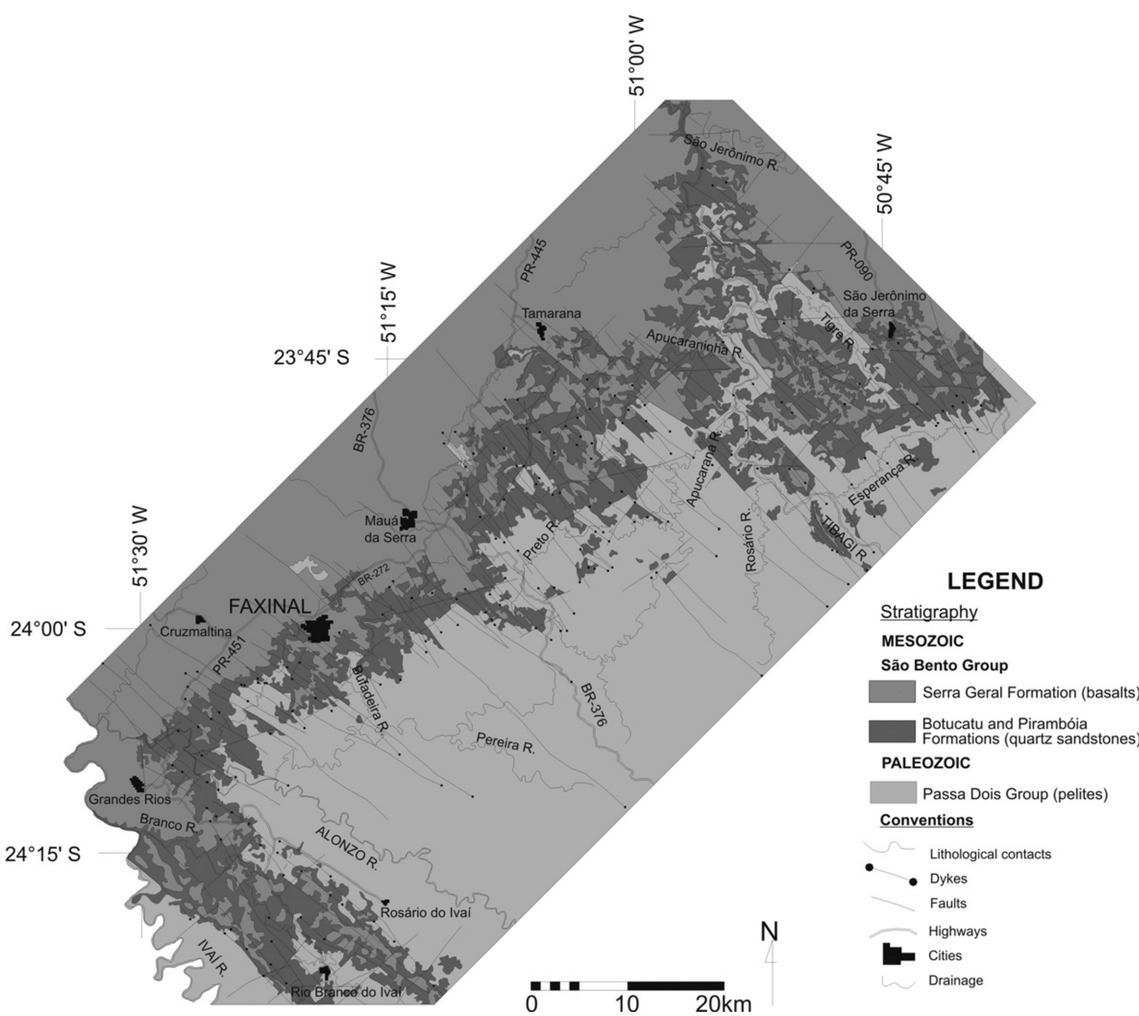

Fig. 2. Geological map of the study area, with faults that delimit lithostratigraphic units.

imagery, provides the main research tool. The pattern, density, and continuity of positive and negative lineaments were interpreted from 1:70,000 aerial photographs (ITC-PR, 1962). The most conspicuous and continuous lineaments were enhanced by filtering. Combined with interpretation of satellite images, these photolineaments mark more deformed zones in each main direction. At outcrop scale, fractures and kinematic indicators, geometry, and filling were described and measured. These data support dynamic fault analysis and discrimination of the stress field for each fault set. Structural data are represented in quadrant form, with dip directions indicated in figure captions. Another research tool, digital terrain modeling (DTM) obtained from the interpolation of contour lines from 1:50,000 and 1:100,000 topographic maps, helps identify major fault zones and compare them with structural compartments against relief and geological maps. A structural contour map of Botucatu Formation was generated by overlaying the DTM and geological maps, which clarified its spatial distribution in relation to major faults and compartments. Aeromagnetometric data were also used to verify the spatial relationship in comparison with geological and photolineament maps.

2. Stratigraphy of São Bento Group

The Pirambóia Formation is composed of friable, fine to very fine-grained, texturally and mineralogically mature sandstones with low-angle cross-bedding. The sets are up to 3 m thick, interrupted by reactivation surfaces. The underlying Rio do Rasto Formation is composed of reddish siltstones and very fine-grained sandstone bodies (Fig. 3). The thickness of the Pirambóia Formation varies in the study area from NE to SW. It is 20 m near São Jerônimo da Serra; there are no outcrops in Tamarana (near the central part of the study area); and it is 20 m in Cadeado Range, 20 km SW. Thickness increases gradually to SW, reaching up to 80 m in Rio Branco do Ivaí. The Botucatu Formation rests in angular unconformity over the Pirambóia Formation, with a constant thickness of approximately 70 m, and can be divided into a 20 m thick torrential facies at the bottom and a 50 m thick eolic facies at the top (Soares, 1975). Intertrapp sandstone bodies up to 20 m thick are common in the base of Serra Geral Formation. The torrential facies is represented by medium- to very coarse-grained, reddish, rounded to subrounded quartz sandstones. Stratification is marked by small-scale trough and low-angle planar cross-bedding, with abundant small angular cobbles of green silty mudstone. This unit rests on the Pirambóia Formation with an irregular surface, with channel-filling and convoluted lamination. The eolic facies consist of fine-grained, well-selected, and rounded red sandstones with medium to large (up to 10 m) trough cross-bedding. The Serra Geral Formation is composed of basalt and porphyritic dacite extrusive bodies up to 50 m thick. It results from fissural volcanism usually accompanied by silicification of underlying sandstones. This unit relates to a series of intrusive, sill-like bodies and, mainly, dolerite dykes over 100 m thick, fitted into faulting planes, which are responsible for important aligned morphostructures. Some dykes cut lower Serra Geral extrusives.

Some authors (e.g., Milani et al., 1994) do not include the Pirambóia Formation in the São Bento Group because of its stratigraphic relationship with the Permian Rio do Rasto Formation. In the present work, Pirambóia sandstones are included in the São Bento Group, even if the strata geometry (Fig. 3) and thickness data show that uplift and erosion of Pirambóia sands preceded Botucatu sedimentation at the axis of Ponta Grossa Arch (Strugale, 2002). The top of the Botucatu formation is time positioned by intercalation of intertrapp eolian sand bodies and first basalt floods. The wide K–Ar ages of Serra Geral basic rocks average 120–130 Ma (Rocha-Campos et al., 1988). More recently, an interval of 10 My was defined for Serra Geral volcanism, between 138 and 127 My

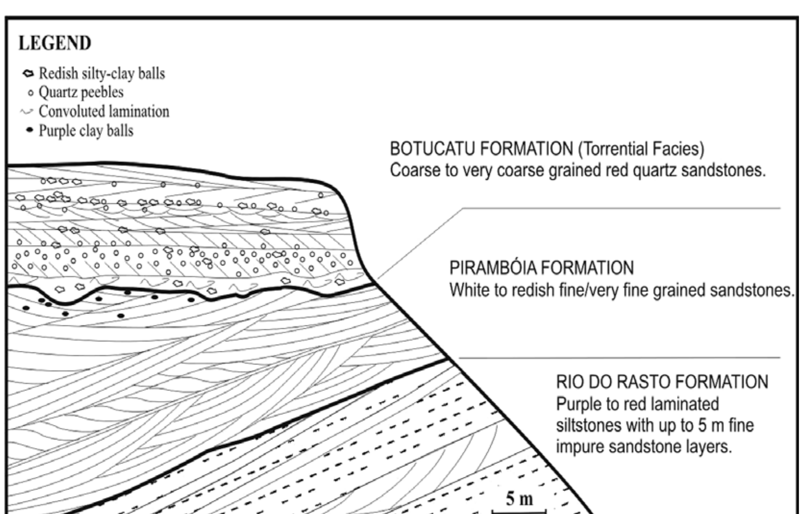

Fig. 3. Contact relationships among Rio do Rasto, Pirambóia, and Botucatu Formations in Serra Fria (PR-090 road, near São Jerônimo da Serra).

(Renne et al., 1992; Turner et al., 1994; Stewart et al., 1996). A Late Jurassic age is estimated for the beginning of Botucatu sedimentation.

3. Structural geology

Structural analysis is based on geometric and kinematic elements observed in fieldwork, regional framework derived from the contour map of the top of Botucatu Formation, DTM, and aeromagnetometric data. Field-based and regional information were integrated through analysis of aerial photographic data. Fault and mapped units distribution, terrain compartments, and morphostructures, such as positive and negative alignments and scarps, were described and correlated. The Riedel terminology (R, R′, Y, and P) for conjugated structures is applied to contemporaneous systematic faults observed in outcrop and images.

3.1. Photolineaments

Photolineaments represent the main set of morphostructures, formed by positive and negative alignments interpreted from aerial photographs, DTM, and Landsat images. Other related morphostructures, such as fault scarps and tilted beds, are also easily observed in images. The main photolineament trends are N40–55W, N40–60E, N–S, and E–W (Fig. 4). The predominant direction is N40–55W, followed by N40–60E. Presence, continuity, persistency, and kinematic indicators in the main photolineament sets, mainly found in the Rio do Rasto and Serra Geral Formations, were investigated. The characteristics of photolineaments of the Pirambóia and Botucatu Formations could not be observed in aerial photographs due to the narrow outcrop areas of these units.

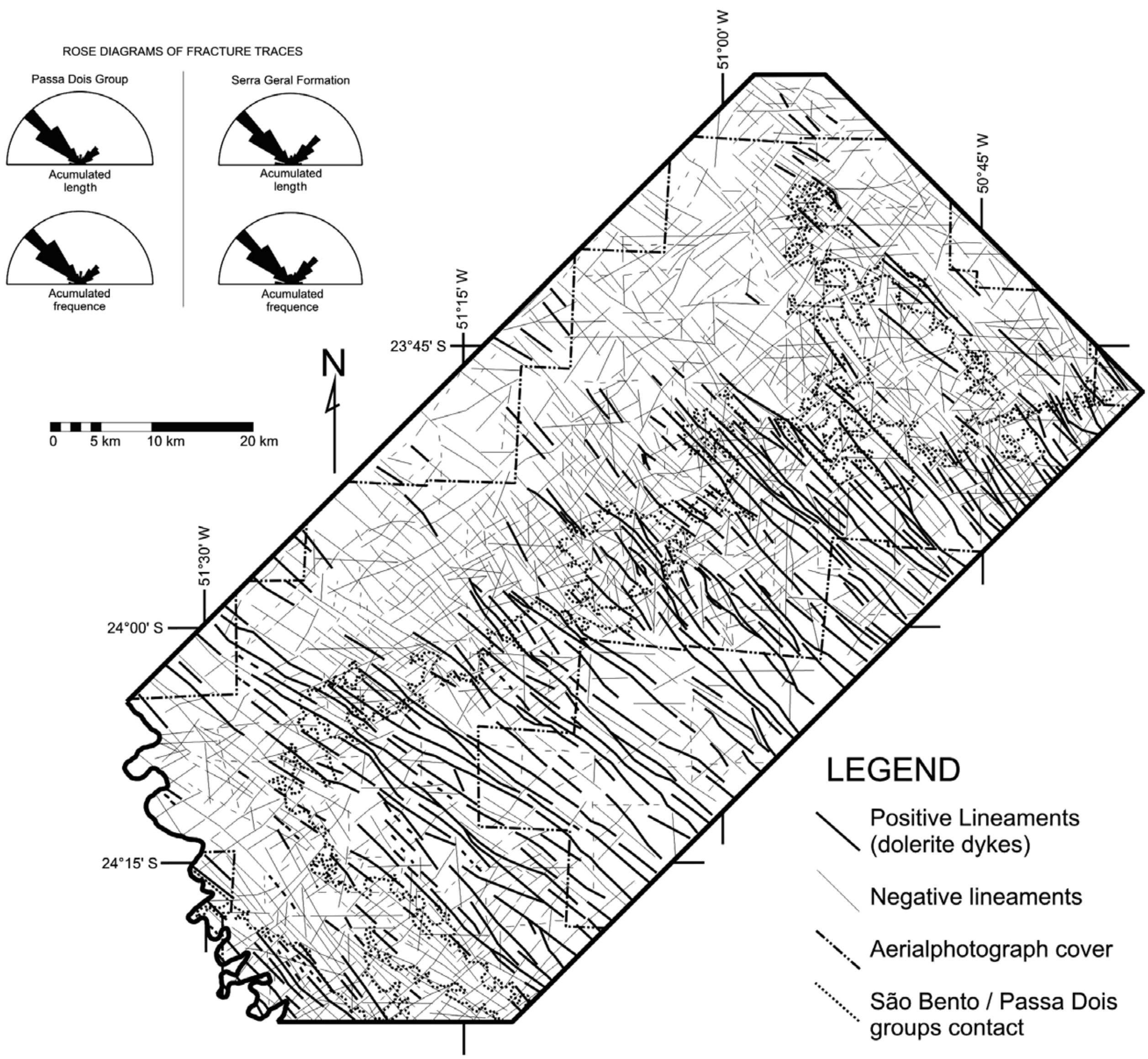

Fig. 4. Filtered negative and positive (dykes) photolineaments, with rose diagrams for major outcropping units (Passa Dois Group and Serra Geral Formation).

3.1.1. N40–55W trend

This trend presents the most continuous lineaments, mainly corresponding to dolerite dykes that fill brittle faults. These structures are well marked in sedimentary rocks of the Rio do Rasto, Pirambóia, and Botucatu Formations, observed as positive and negative alignment sets up to 20 km long. Significantly high concentrations of dykes and negative alignments are identified in aerial photographs, which can be grouped into fault zones (NW–SE fault zones) that behave like deformation belts (Fig. 5). The fault zones present a slight divergence, ranging from N40W to N55W toward the central part of the basin. Different geometries in fault zones are observed due to their relative position with the Ponta Grossa Arch axis and Rio Alonzo and São Jerônimo-Curiúva structural-magnetic alignments. Fault zones located along this axis (Incrão, Mauá da Serra, and Faxinal) are branched, whereas those adjacent to the structural-magnetic alignments at the border (e.g., Rio do Tigre, Tamarana, and Rio Pereira) tend to be straight. Along the fault zones of Faxinal, Cruzmaltina, and Rosário do Ivaí, some dykes extend for more than 50 km toward the basalt cover and coincide with the Rio Alonzo Alignment area. Field work, aerial photographs, and Landsat TM7 images show that dykes in the Serra Geral Formation are mainly planar, unlike those intruded in underlying sedimentary units. Dykes do not cross the porphyritic dacite extrusives at the top of the Serra Geral Formation (e.g., Faxinal–Cruzmaltina region). Other

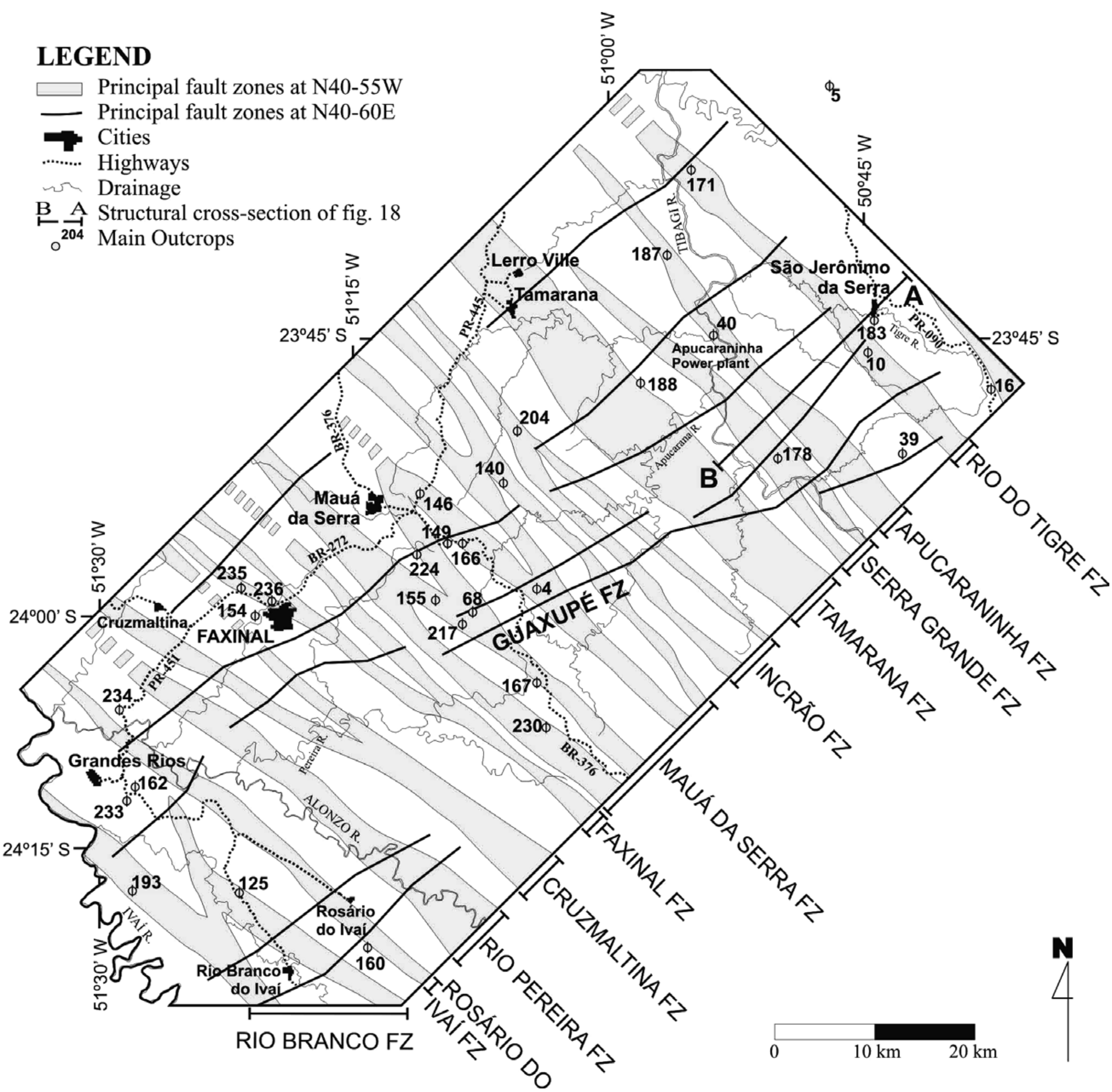

Fig. 5. Structural framework of study area, containing NW–SE and NE–SW fault zones related to Ponta Grossa Arch and Guaxupé Fault Zone (N60E) added to main N40–60E fault traces (Strugale et al., 2002), with the labels of outcrop sites mentioned in the text.

NW–SE fault zones extend for several kilometers as negative alignments (e.g., Tamarana fault zone) toward the basalt cover.

3.1.2. N40–60E trend

The N40–60E faults are more scattered than NW–SE fault zones. The most prominent corresponds to an extension of the Precambrian Guaxupé fault zone into the Paraná Basin (Fig. 1) that crosses the study area as a fault zone of about 10 km width (Figs. 4 and 5). This trend of photolineaments shows different orientation in pelites of the Rio do Rasto Formation and in basic volcanic rocks of the Serra Geral Formation. In the former, N60E photolineaments are curve-planar and present discontinuous deformation revealed by localized branching zones. However, NE–SW sets are preferentially oriented N40–50E in basalts, in which they mark straight photolineaments. They concentrate in two splays branching from north of the Guaxupé fault zone (Fig. 5). Another important set of NE–SW lineaments occurs in the southern part of the area, in Rio Branco do Ivaí, and could reflect the Jacutinga fault zone near Cândido de Abreu, about 20 km to the south.

3.1.3. N–S and E–W trends

These trends present the largest spacing between lineaments (mean distance 6 km), but overprinted features related to other directions are also observed. The main features consist of planar to slightly curved traces and sets of continuous (E–W trend), or discontinuous and short lineations with steps or *en echelon* geometry in some places (N–S trend). The E–W fractures concentrate north of parallel 23°45′S, in some cases promoting local steps in relief, which suggests neotectonic activity (Strugale et al., 2004). The N–S fracture zones are more regular than their E–W counterparts; the best example is the set that controls the Tibagi River Valley in the eastern portion of the study area (Fig. 5).

3.2. Structural compartmentalization and spatial distribution of the Botucatu Formation

In the study area, structural compartments are bounded by faults, either completely or partially, that represent fault-blocks. At local scale (up to 10 km), the blocks are limited by N40–55W brittle shear zones crossed by N40–60E major faults, each of which shows different magnitudes of deformation (Fig. 5). At regional scale (greater than 10 km), northeast, central, and southwest morphotectonic blocks exert influence on the configuration of altimetric isolines along the contact of the São Bento and Passa Dois groups and at the top of the Botucatu Formation (Fig. 6). The compartments are defined by N40–55W and N40–60E faults, the interaction of which generated a series of rhomboedral blocks that define the first-order structural compartments of the study area. The same pattern is observed at regional scale in Fig. 1, in which the central-northern Paraná appears to have been affected by widespread N40–55W fault zones that correspond to structural-magnetic alignments described by Ferreira (1982a,b) and by N40–60E fault zones (Guaxupé and Jacutinga). The NE–SW fault zones in the Paraná Basin are extensions of the main basement transcurrent faults (Ribeira Belt). Scissor faults are responsible for alternating structural highs and lows in the geologic map (Fig. 2) and delimit the NW–SE brittle shear zones. They mark more deformed 3–5 km wide areas, except for the Tamarana fault zone, which is 8 km wide and presents a smaller thickness and higher dyke concentration. Structural highs delimited by kilometer to 10-kilometer N40–55W faults that extend toward the São Bento Group are typical of Rio do Rasto Formation outcrops. Such features are more clearly observed between Tamarana and Mauá da Serra (Fig. 2). Rio do Tigre Horst (Strugale et al., 2004), west of São Jerônimo da Serra (Fig. 18), is another example of a structural high that tends to coincide with a brittle shear zone, like other similar structures.

The main pattern of structural contours of Botucatu Formation altimetry, relief (Figs. 6 and 7), and distribution of lithostratigraphic units (Fig. 2) is controlled by the regional northeast, central, and southwest blocks (Fig. 6), which are separated by the Rio Pereira and Tamarana fault zones that approximately coincide with the Rio Alonzo and São Jerônimo-Curiúva structural-magnetic alignments, respectively. Deflections of structural contour curves and geologic contacts are the main delimitation criteria for the central block compared with the northeast and southwest ones. Although altimetry and structural contour gradients are particular to each block, the same cannot be said of transition zones. The higher contour curves of both NW and NE boundaries of the central block mark altitudes of 650 and 750 m, respectively. The central block is characterized by its higher relief (up to 1300 m) and Botucatu Formation outcrop altitudes compared with those of adjacent blocks (Fig. 7). No significant changes in structural contour or altimetry in the Botucatu Formation are observed across the major N40–60E faults, except in the Guaxupé fault zone, which exerts some influence on these elements.

In the Paraná Basin, the NE–SW basement faults usually exhibit reactivation features (Soares, 1992; Rostirolla et al., 2000, 2003), and the interaction between these faults and NW–SE structures originates structural highs such as the Quatiguá, Pitanga, Anhembi, and Piratininga domes. In the study area, at least two similar structural highs show circular to rhomboedral features, where the Rio do Rasto Formation is surrounded by São Bento Group units. These highs are located in the Cadeado Range region, about 10 km east of Mauá da Serra (Fig. 2), where the Guaxupé and Mauá da Serra fault zones intersect.

3.3. Aeromagnetometry

Ferreira (1982a,b) proposes a structural framework for Ponta Grossa Arch based on magnetometric data analysis

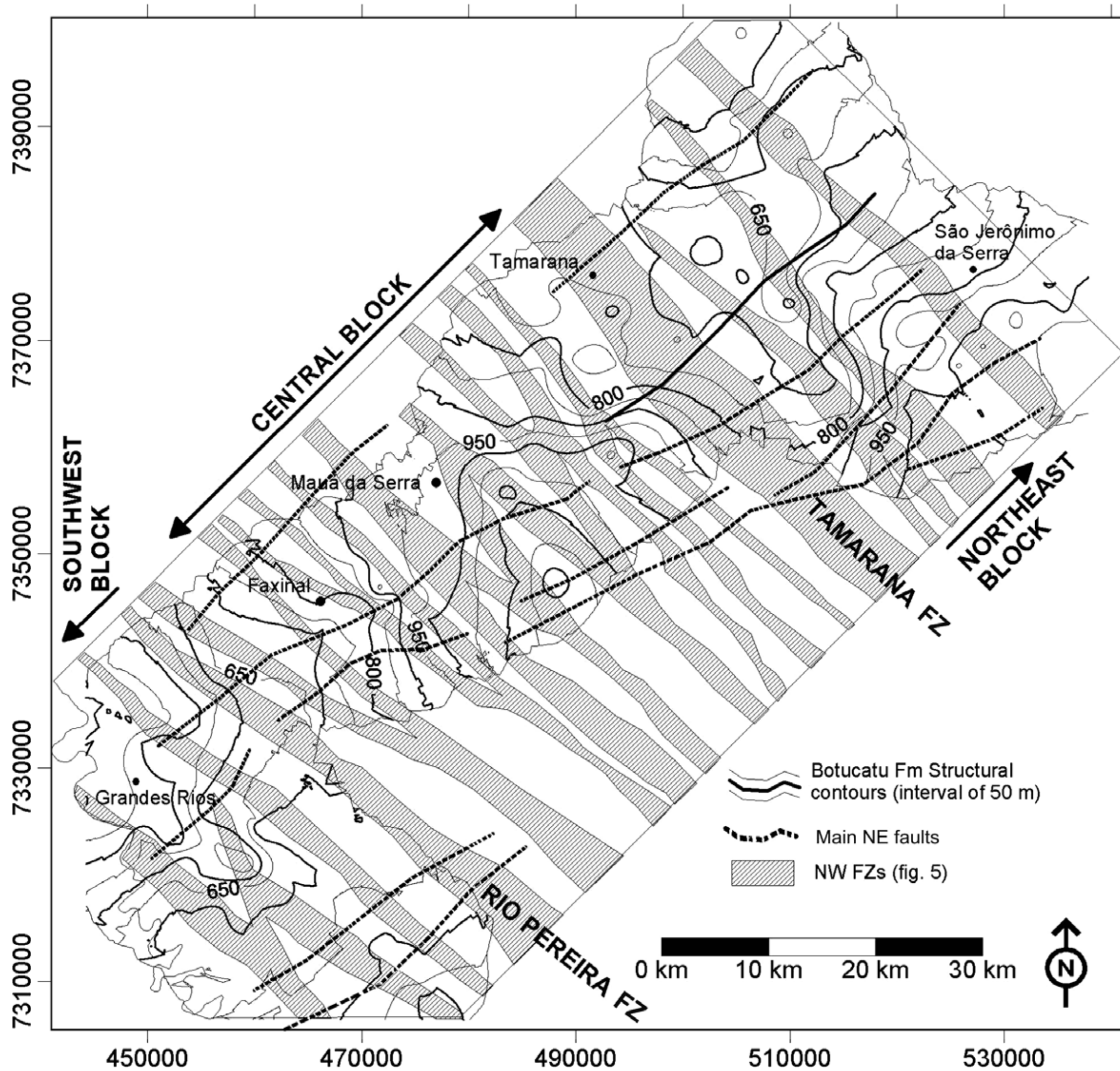

Fig. 6. Structural contour map of top Botucatu Formation, including the NW–SE fault zones and the most conspicuous sets of N40–60E faults.

along major NW–SE fault zones filled with dolerite dykes. Four structural alignments were distinguished: Guapiara (northern limit), São Jerônimo-Curiúva and Rio Alonzo (central region, axis) and Rio Piquiri (southern limit), as simplified in Fig. 1. The structural-magnetic alignments extend up to 600 km, with a maximum width of 100 km in the central part. The study area is indicated in Fig. 8, on the partial magnetic map of Paraná (Ferreira and Portela Filho, 2001). The aeromagnetometric data used were collected as part of the Iguaçu River and Ivaí River aerogeophysical projects. They were acquired in, respectively, 1980 and 1981 through a CESP/IPT (Paulipetro) partnership. The mean flight heights were 500 m (Iguaçu River) and 450 m (Ivaí River), the line separation was 2000 m, and flight direction was N–S. The data were provided to Universidade Federal do Paraná (UFPR) in digital form by Petrobras (Brazilian state oil company), already processed for positioning, leveling, correction of diurnal variation, and main earth field removal (IGRF – International Geomagnetic Reference Field). Data were first assessed and interpolated using the minimum curvature method (Briggs, 1974) following a regular grid of 500×500 m cells selected after several statistical testing and visual inspection phases. Some artifacts were present along the flight lines. To remove or smooth such noise, several micro-levelling techniques (Minty, 1991) were tested, and the bidirectional method was chosen (Geosoft, 2001).

3.3.1. *Horizontal gradient, amplitude, and phase of analytic signal*

Since the early 1970s, analytical methods based on horizontal and vertical gradients (derivatives) have been developed that now represent important tools for determining geometric parameters such as location (mapping), delimitation, and depth of bodies able to cause potential field anomalies (Hsu et al., 1996). The zero-order total horizontal gradient is the vector that results from combination of the first horizontal derivatives along the x and y directions, as in:

$$H(x,y) = [(G_x)^2 + (G_y)^2]^{1/2}, \tag{1}$$

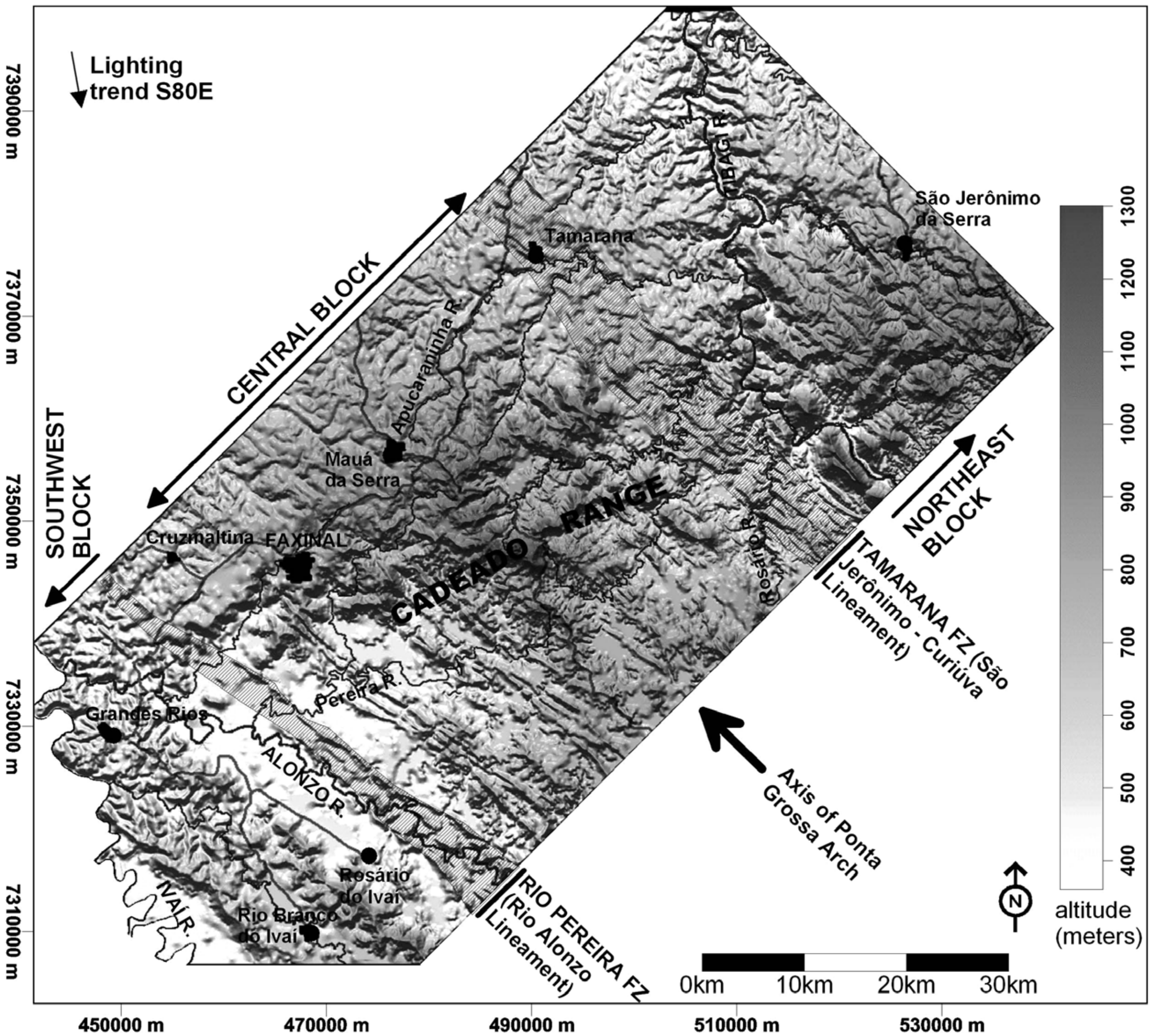

Fig. 7. Digital terrain model (DTM).

where $G_x = \mathrm{d}G/\mathrm{d}x$ and $G_y = \mathrm{d}G/\mathrm{d}y$ are horizontal derivatives of the magnetic field G anomaly. In general, the horizontal gradient indicates sudden changes in the magnetic field, which facilitates mapping.

The analytical signal is a complex function, usually employed in magnetic mapping (Hsu et al., 1998; Bastani and Pedersen, 2001). One of the main advantages of this method, in addition to allowing body delimitation, is its independence with respect to the magnetization direction, such that a body with a specific geometry and magnetic susceptibility will show the same analytical signal at any latitude. The amplitude of a zero-order (simple) analytical signal (Nabighian, 1972, 1974) is represented by the following equation:

$$|A(x,y)| = [(G_x)^2 + (G_y)^2 + (G_z)^2]^{1/2}, \tag{2}$$

where $G_z = \mathrm{d}G/\mathrm{d}z$ is the first vertical derivative of G; and G_x and G_y are as previously defined.

The zero-order analytical signal phase that delineates shallow magnetic sources (high spatial frequency) is defined by the angle between imaginary and real vectors of the same order of analytical signal, the resultant ratio of the first vertical derivative, and the horizontal gradient:

$$\Phi(x,y) = \mathrm{arctg}(G_z)/[(G_x)^2 + (G^y)^2]^{1/2}. \tag{3}$$

These methods were applied to the study area, considering the residual magnetic field grid in Fig. 8. From several maps generated, the residual magnetic field (database) and the horizontal gradient maps selected are presented in Figs. 9 and 10, respectively. They were pseudoilluminated using a 45° sun elevation angle and include a delineation of NW–SE fault zones and NE–SW structures. The E–W artifacts are observed mainly in Fig. 10, especially near UTM 7340000, as a link reflection of the two aerosurveys used. Fig. 10 also shows other artifacts in the northern portion of the study area, such as near UTM 7370000. Other

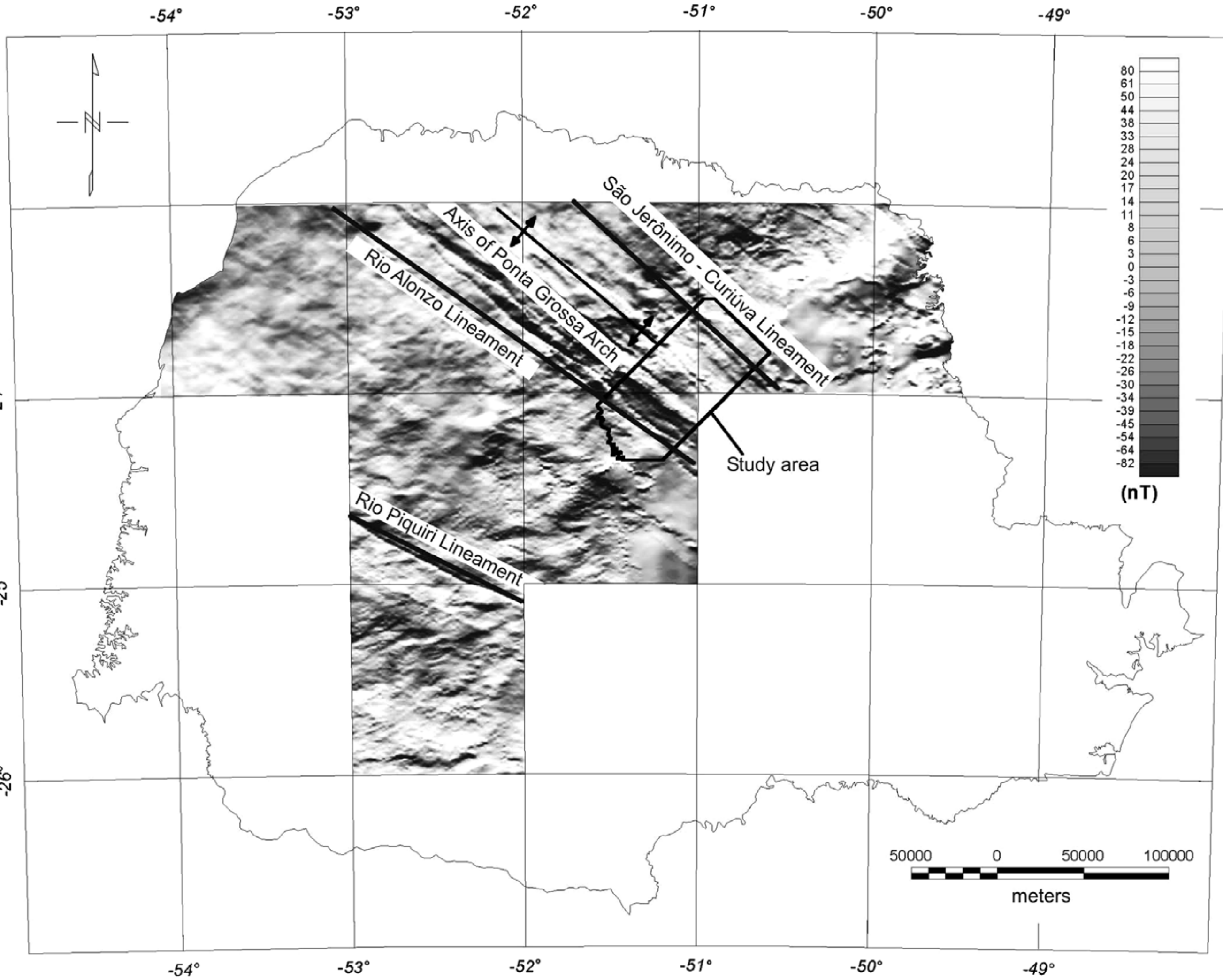

Fig. 8. Partial magnetic map of Paraná covering most of the study area (Ferreira and Portela Filho, 2001).

artifacts also can be noticed along the flight line (N–S), especially in the southwestern portion of the study area. Such artifacts are due to the reduced dimensions of the area compared with the original grid size, which was leveled and micro-leveled at regional scale (1:1.000,000). The maps in Figs. 9 and 10 show that the most prominent magnetic alignments in the study area are oriented N40–55W, the main orientation of photolineaments and dolerite dykes. A remarkable coincidence of magnetic alignments and NW–SE fault zones is also observed, especially for the Apucaraninha and Rio Pereira fault zones, which delimit the central part of the Ponta Grossa Arch. They coincide with São Jerônimo-Curiúva and Rio Alonzo alignments in the northeastern and southwestern portion of the study area, respectively. The horizontal gradient map in Fig. 10 portrays the spatial relationship between magnetic anomalies and NW–SE fault zones between the previously mentioned structural-magnetic alignments. The coincidence of ramifications of NW–SE fault zones and magnetic anomalies is remarkable in the central part of Ponta Grossa Arch, near Cadeado Range. The profusion of dolerite dykes in Fig. 4 is not perfectly characterized in magnetic maps because of the flight height (500 m) and sampling space flight lines (2000 m) used. These factors resulted in resolution loss and even the lack of a geophysical record of thin dykes observed in the field and aerial photos. Ussami et al. (1991) demonstrate this problem by comparing terrestrial and aerial magnetometric data from the dyke swarm at Serra da Fartura (SW of São Paulo State) within the Guapiara Alignment (the northern limit of Ponta Grossa Arch; Ferreira et al., 1981). The NE–SW faults are also observed on magnetic maps, though not as clearly. They consist of alignments related to gradient breaks and usually are limited by more conspicuous NW–SE structures. The four main sets of photolineaments in this structural direction can be visualized on magnetic maps, especially the Guaxupé fault zone.

3.4. Descriptive structural analysis

Field structural data and photointerpretation provide a great amount of linear and planar structural information, interpreted in terms of geometry and kinematics. Discontinuous structures represent the main set of faults, but

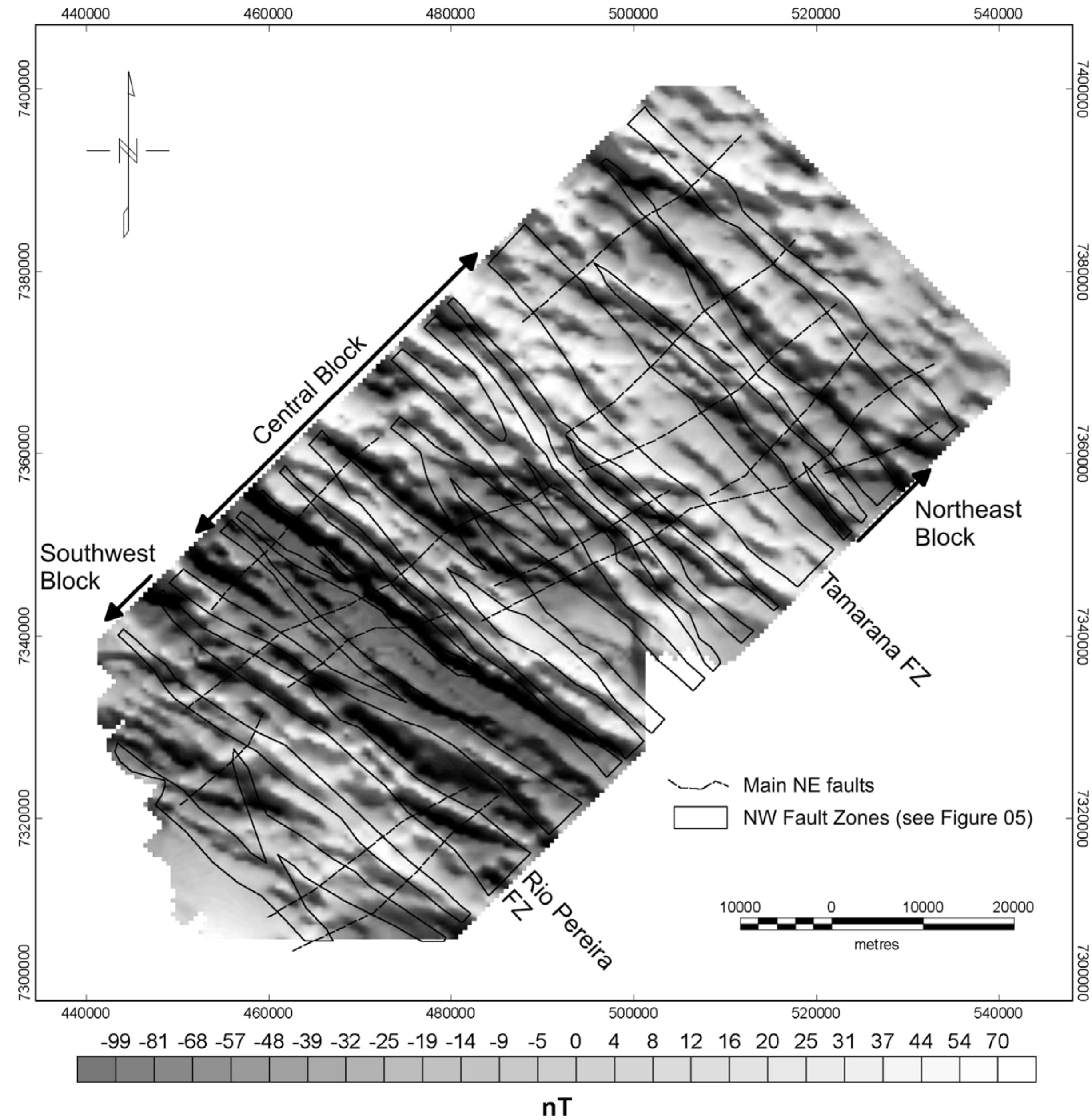

Fig. 9. Residual magnetic map of the study area.

some occur as continuous deformation bands in sandstones. The disposition of faults reflects a regional non-continuous and non-penetrating deformation.

3.4.1. Planar structures

Joints are the most abundant planar structures observed at outcrop. The total rose diagram (more than 1100 planes) does not show a preferential orientation. However, patterns are more consistent when joints are grouped by lithoestratigraphic units. In sandstones, for instance, joints close to a N50W mode prevail, whereas joints approximately N–S are virtually absent. Depending on the lithology, fractures vary mainly in geometry and filling. In sandstones, fractures tend to be planar. In extrusive basalts and dykes, they are planar to undulating, usually filled with fibrous or euhedral calcium carbonate, manganese oxide, and, locally, pyrite.

Faults are highly diverse in geometry and kinematics (Fig. 11) because not only they distinct rocks, but they also show vertical and horizontal displacements that vary from a few centimeters (local) to more than 100 m (regional). In some cases, fault contacts observed in aerial photos indicate vertical displacement, as in the fault that marks the contact between the Rio do Rasto and Serra Geral Formations (Fig. 12). Regional faults are best observed in aerial photographs, because of the control on river valleys, fault scarps, and lithological contacts. They extend for more than 10 km and form

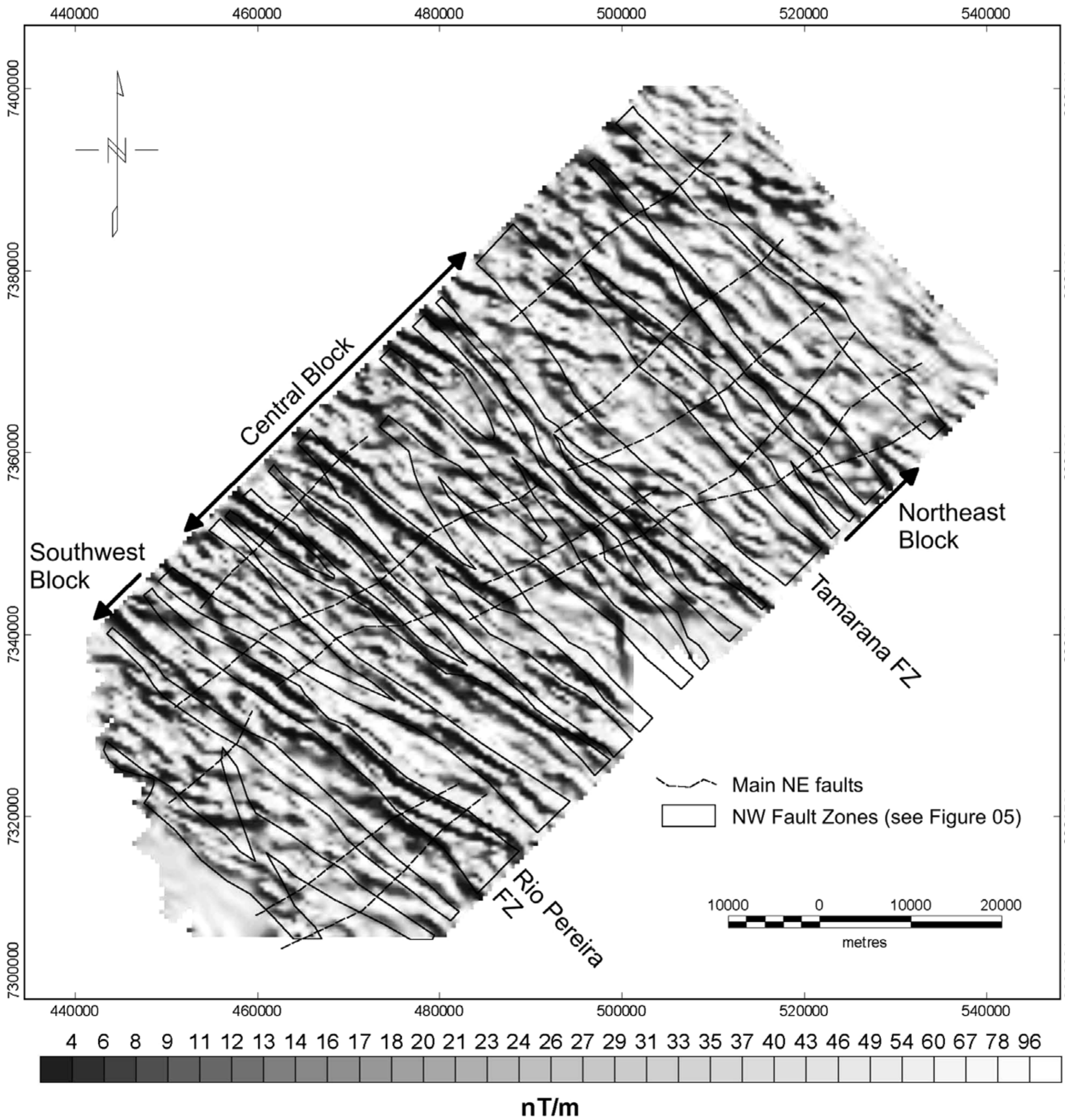

Fig. 10. Zero-order total horizontal gradient map of the study area.

straight to undulated planes. Faults striking N40–55W indicate important displacements in the contacts between the Pirambóia and Botucatu Formations (Fig. 2). Strike-slip and extensional faults are predominant (Fig. 11), whereas reverse faults are sparse and found near the arch axis. However, a decrease of vertical displacement magnitude in most of NW faults is usually observed toward the NW. The geologic map (Fig. 2) shows that large, NW regional faults usually present major displacements when crossing the sedimentary rocks but disappear when they reach the Serra Geral Formation flows, which indicates rotational or scissor-like faulting. These faults are usually located at the borders of NW–SE fault zones, such as the fault on the northeastern border of the Tamarana fault zone (Fig. 12).

The most common kinematic indicators in faulted sandstone layers are steps and groove lineations (Fig. 13), which reflect deformation in uppermost crustal levels. However, the presence of deformation bands implies considerable confining pressure, occurring when the Botucatu Formation reaches deeper levels. Syn-depositional microfaults also were observed to affect some stratigraphic levels of the aeolian facies of the Botucatu Formation and intertrapp sandstones (Fig. 13B). Deformation bands are restricted to the sandstones and sometimes exhibit kinematic indicators as sigmoids, flexures, and steps. In igneous rocks, kinematic indicators are usually slickenside or fiber growth lineations and, rarely, en echelon fractures (Fig. 14). The predominant geometry is undulated to planar, which in quarries can be mistaken

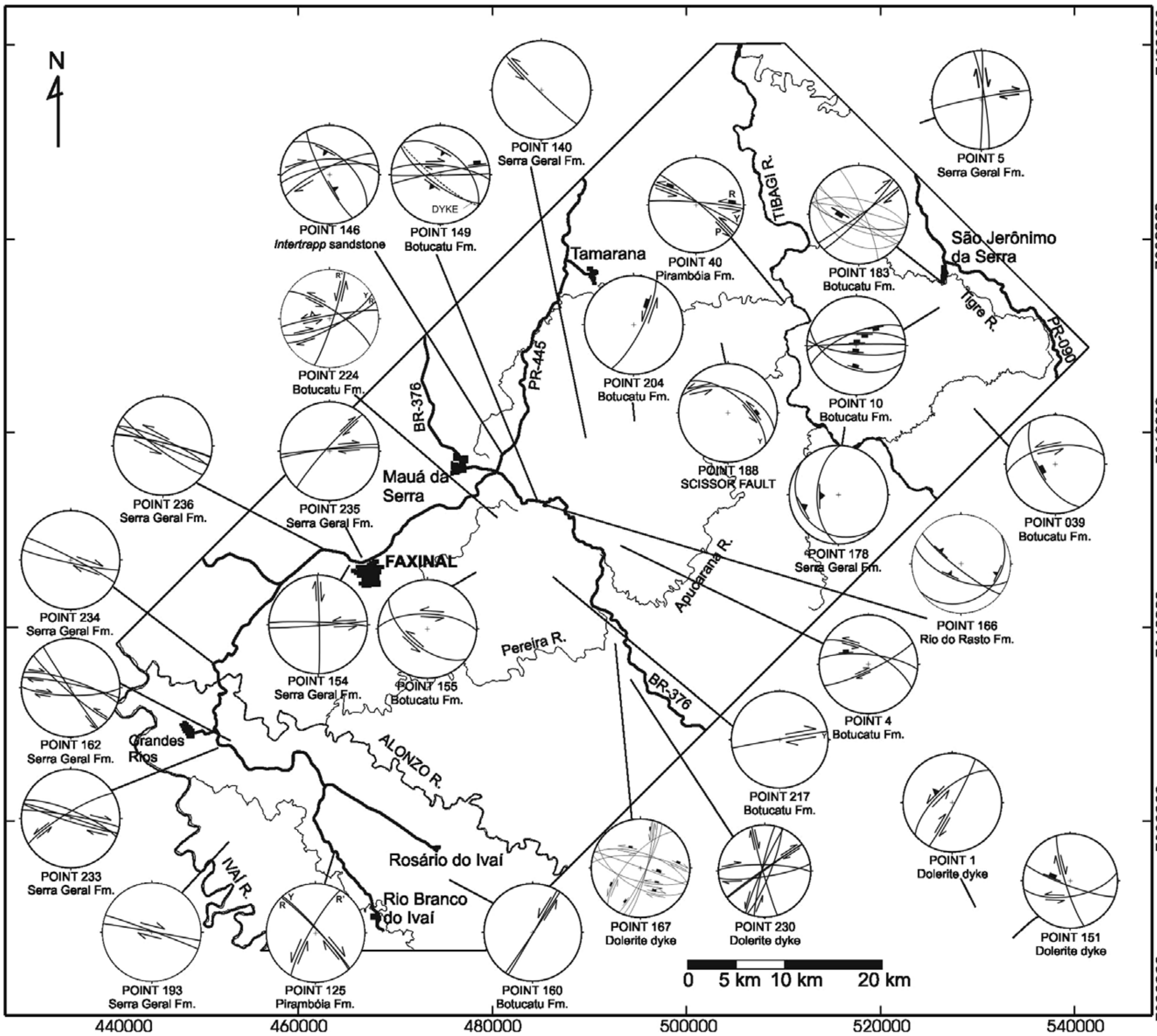

Fig. 11. Cyclographic projections with the kinematics of field-observed faults (Schmidt net, lower hemisphere).

for columnar joints. For this reason, chronological relationships among faults at outcrops of basic igneous rocks are difficult to establish.

Deformation bands are the most important structural elements in sandstones. They strike exclusively N50W and show strong silicification (Fig. 15), whose dimensions are controlled by the amount of displacement and deformation. Two outcrops contain branching fault zones with 5 m wide deformation bands related to the borders of the Mauá da Serra and Apucaraninha NW regional faulted belts. These more developed bands show Riedel R, P, and Y fracturing directions, which compose a branching fault pattern. Deformation bands show particular characteristics when observed in thin sections, which can be related to fault kinematics and deformation magnitude. Fig. 16 shows broken grains at the border of the band with some of them immersed in an iron hydroxide matrix in more deformed zones, and aeolian bedding preserved in less deformed ones. A thin section from site 40 shows only a highly deformed zone with intense grain breakage. Grains are faceted and sometimes comminuted in gouge zones. Deformation bands are formed by tectonic shearing in porous sandstones, in which deformation is accommodated by pore collapse, grain scale fracturing, comminution, and cataclastic flow (Aydin (1978) in Davis et al. (1999)). During band formation, brecciation allowed fluid percolation until the start of the gouge stage, when permeability dropped down, giving an important indication of hydrocarbon migration paths in oil-bearing basins (Magnavita, 2000). After shearing, dissolved species precipitated, and most bands were filled by siliceous or iron hydroxide. The growth of deformation bands occurs in specific fluid pressure and lithostatic conditions that are not observed at or near the surface. The plasticity of sandstone increases exponentially with the confining pressure (Donath (1970) in Billings (1972)), which explains the

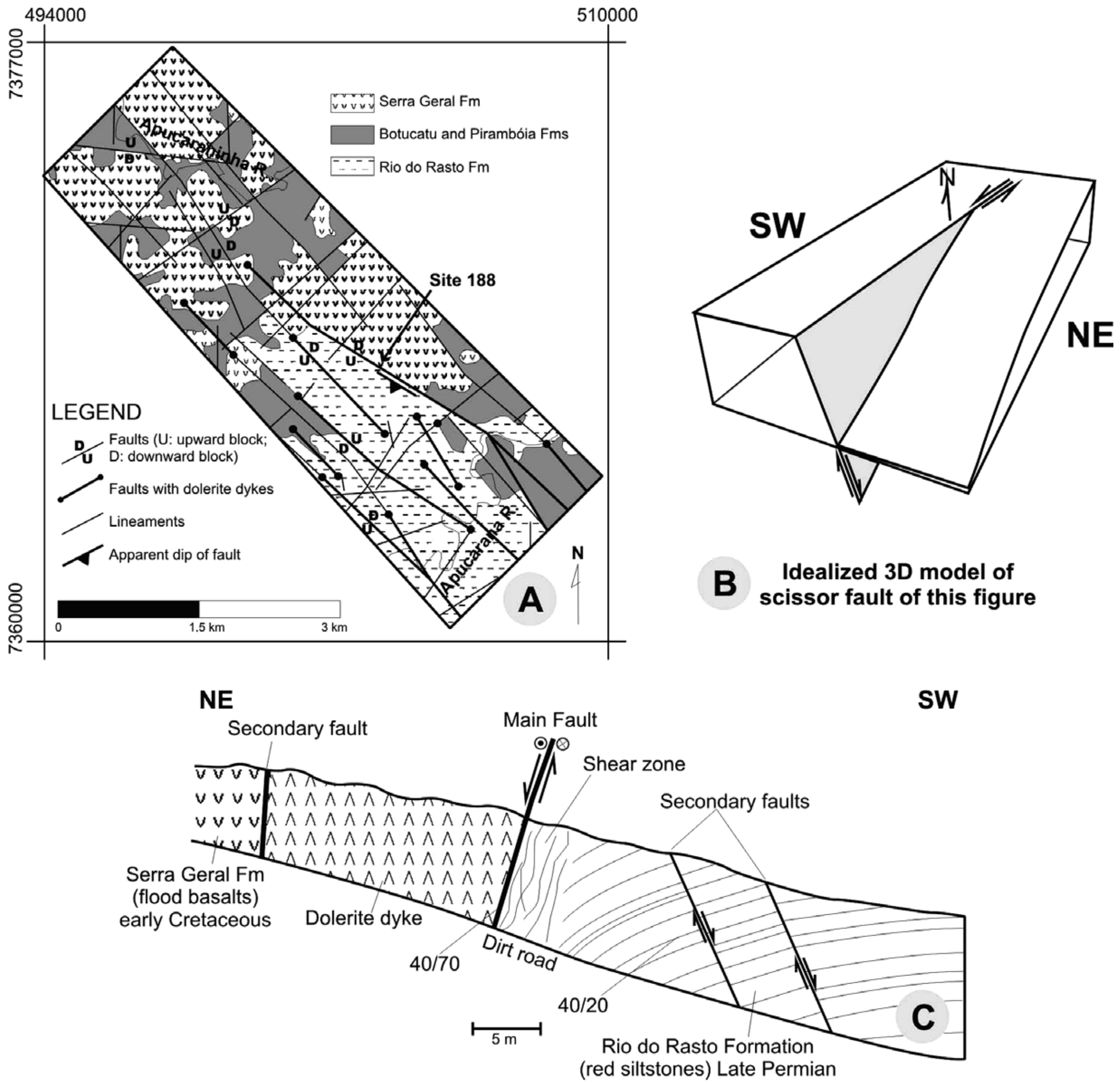

Fig. 12. (A) Map aspect of scissor-like faults. (B) Schematic representation of the geometry of faults. (C) Fault plane in outcrop (site 188) with a vertical displacement of at least 100 m; slickenside lineations indicate left-lateral reactivation of the main fault.

presence of continuous structures such as branching and sigmoidal patterns in the most developed bands. Formation water in permeable sandstones is another factor that increases plasticity through strain softening. The conjunction of all these factors indicates that the deformation bands were tectonically generated at a time when the burial by Serra Geral Formation basalts was already present.

3.4.2. Linear and filling structures

Linear structures observed in outcrops consist of slickenside lineations and troughs. Slickenside lineations present shearing-generated steps, with fibers grown contemporaneously with deformation (Fig. 17). Euhedral carbonate is observed in several locations and planes with slickenside lineation, which might indicate an extensional event after shearing by mineral precipitation from percolating meteoric water, which cannot be time positioned. Fractures filled with carbonate are observed in three main directions – N50W, N20E, and N70W–and are similar to fibrous or euhedral carbonate. In extensional branching faults (Fig. 14C and F), the presence of such carbonate concentrations as centimeter-size crystals is common in pure extensional domains of fault zones.

3.5. Kinematic structural analysis

This stage of structural analysis was conducted on the basis of outcrop kinematic indicators, their temporal relationships, and photogeological elements. Due to the amount and diversity of structural data, faults are described in relation to their generating events. The dynamic structural analysis reveals that the fractures in the study area resulted from two time-distinct deformation events named D1 and D2.

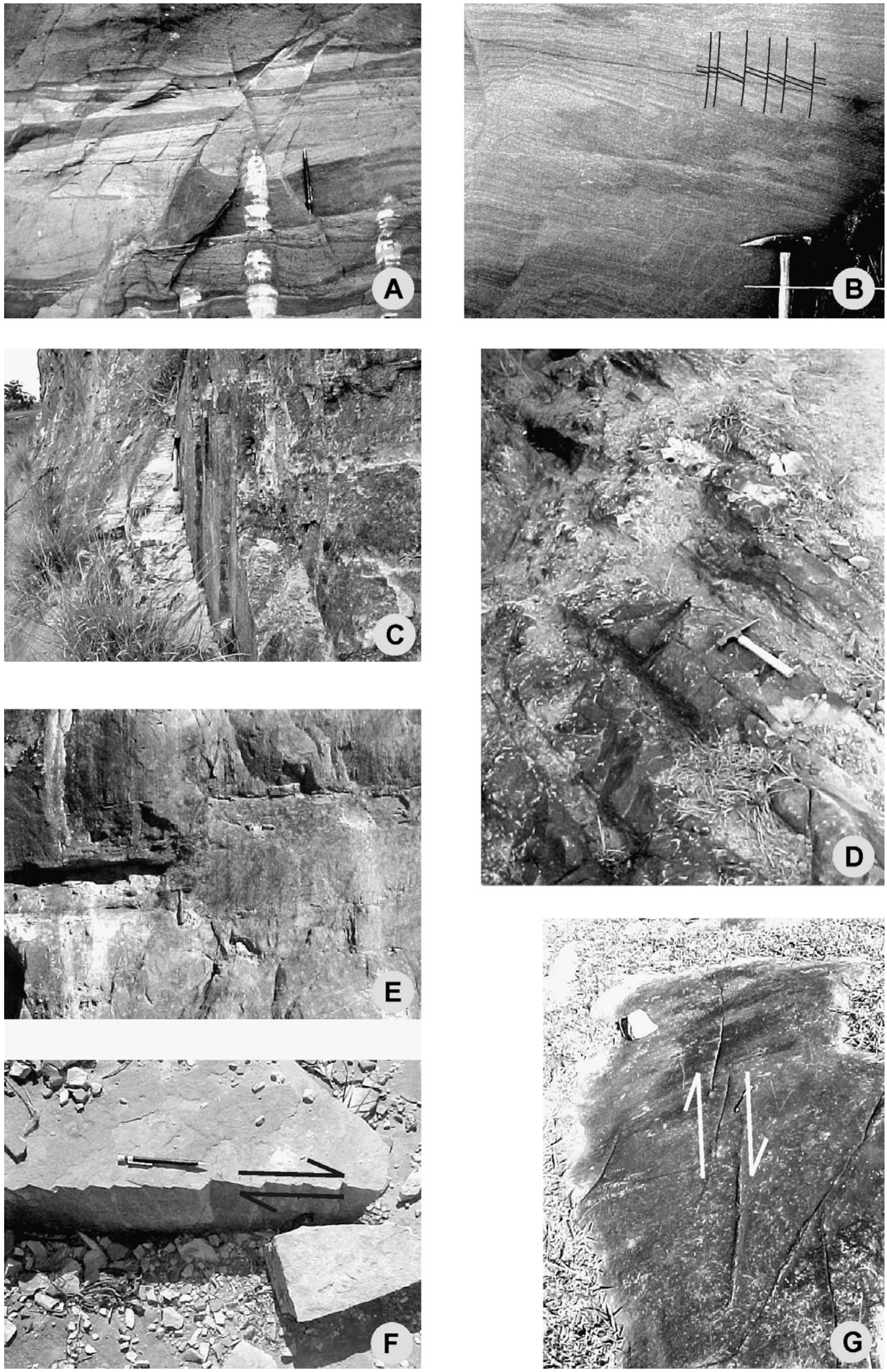

Fig. 13. Discontinuous faults in Pirambóia and Botucatu sandstone outcrops. (A) Normal faults (240/60) in the torrential facies of Botucatu Formation (site 39). (B) Syn-depositional microfaults in intertrapp sandstone, Cadeado Range (site 68). (C) En echelon fractures in Pirambóia Formation (site 125, Grandes Rios to Rio Branco do Ivaí road), indicating right-lateral movement (plane 48/84). (D) 150/85 shear zone in aeolian sandstone (Botucatu Formation, site 171). (E) Normal fault (217/80) in the torrential facies of Botucatu Formation, near São Jerônimo da Serra (site 183). (F and G) Plane view of en echelon fractures (150/75, right-lateral) in silicified sandstone of Botucatu Formation (site 224, Cadeado Range).

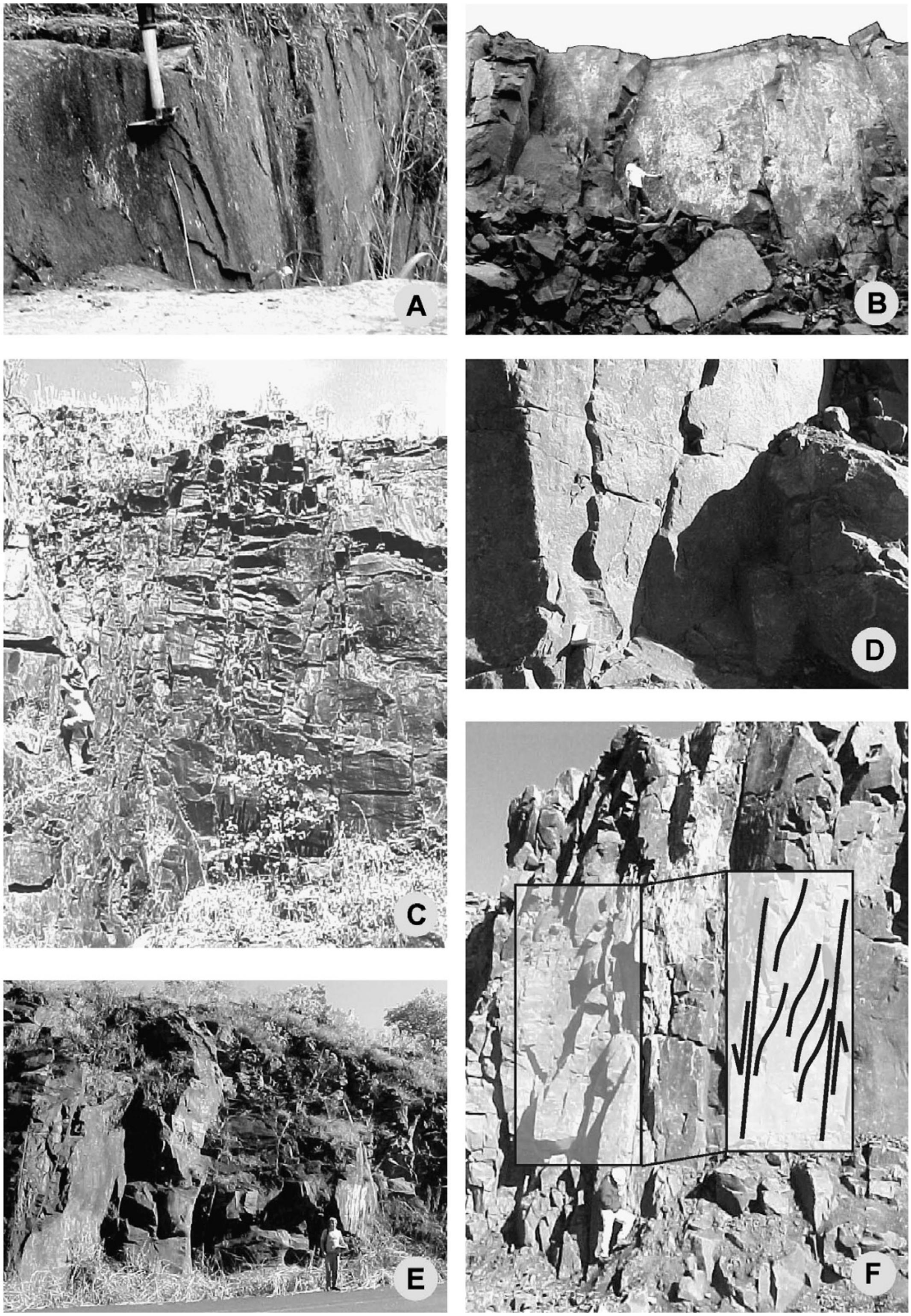

Fig. 14. Faults in outcrops of Serra Geral Formation and basic intrusive rocks. (A) En echelon fractures on left-lateral normal faults (176/88) in porphyritic dacites (quarry in Faxinal, site 154). (B) Fault plane (112/85) filled with euhedral calcite in basalt (site 162). (C) Normal E–W fault zone in dolerite dyke (railway, site 167). (D) En echelon fractures (294/84) on left-lateral fault in a dolerite dyke (CESBE quarry, site 230). (E) Undulated set of fractured (main strike 91/88) in PR-090 road (site 5). (F) E–W fault zone with sigmoidal geometry in CESBE quarry (site 230).

3.5.1. Previous discontinuities

Previous discontinuities in the Permian section propagates deformation to the upper units. Several tectonic events, such as fault reactivation and neoformation, influenced Paraná Basin evolution. The main structures of the basin result from reactivation of basement weakness zones

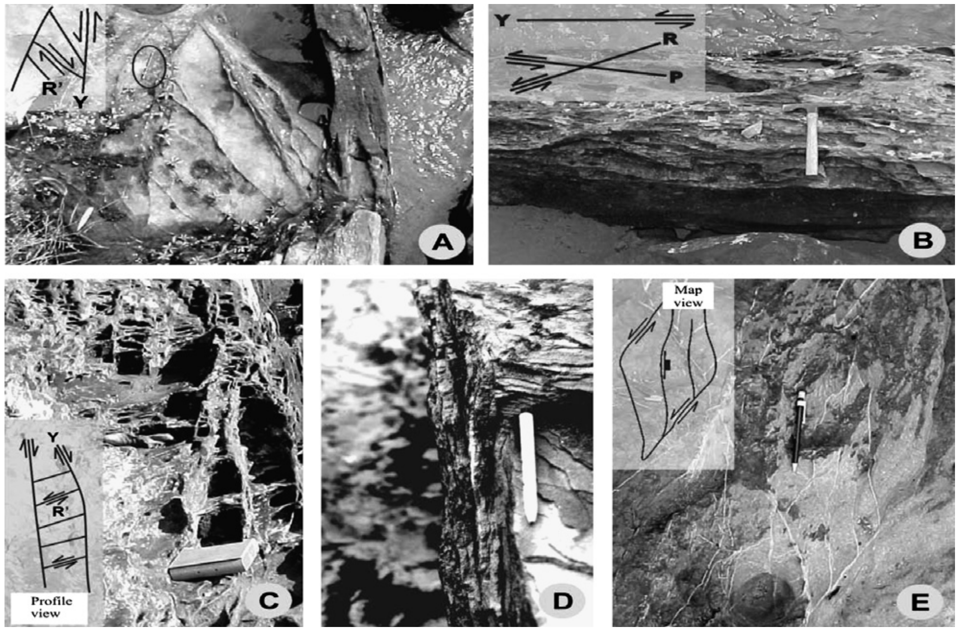

Fig. 15. Deformation bands in sandstones of Pirambóia and Botucatu Formations. (A–C) Deformation bands on left-lateral normal 24/85 fault zone in Pirambóia Formation, near Apucaraninha Hydroelectric Power Plant (site 40). (D) Left-lateral curvilinear deformation bands (35/88) in aeolian Botucatu sandstone (site 4). (E) Milimetric deformation bands in Botucatu sandstone (site 187), indicating pull-apart with down-dip faulting at 190/89.

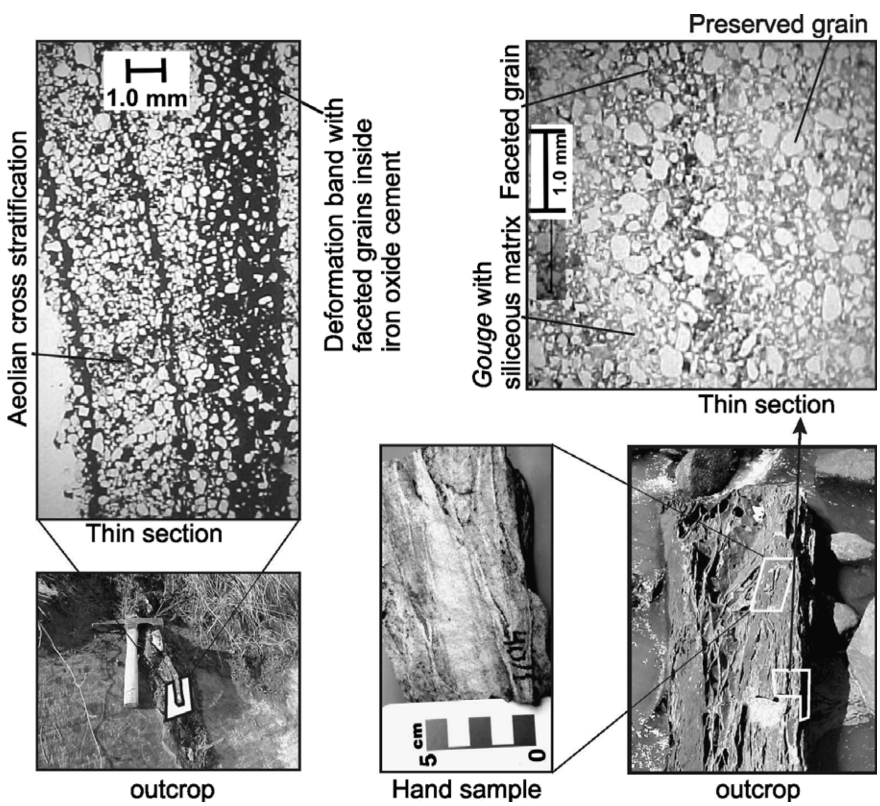

Fig. 16. Photomicrographs of deformation bands. (Left) Deformation band oriented 150/80 in aeolian Botucatu Formation (site 4). (Right) Gouge zone in deformation band in 24/85 left-lateral fault at Apucaraninha Hydroelectric Power Plant (Pirambóia Formation, site 40).

due to stress propagation related to plate-border orogenic events. The main reflections of this reactivations are the NE–SW faults (Soares, 1992; Rostirolla et al., 2000), accelerated subsidence, and extensive erosion cycles in the basin (Milani and Ramos, 1998). In the study area, Guaxupé fault zone reactivation resulted in a set of branching N60E faults, well characterized by morphostructural features. The Jacutinga fault zone, which is parallel to

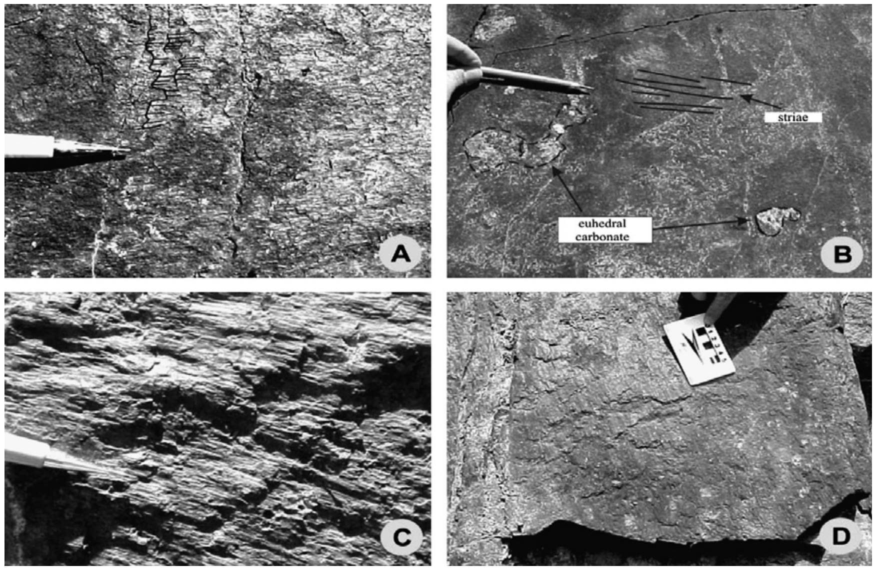

Fig. 17. Faults with fibrous carbonate constituting linear kinematic indicators in Serra Geral basic rocks. (A) Slickenside lineations in fibrous carbonate in 349/86 right-lateral fault (site 5). (B) Grooves in rocks and later euhedral carbonates (site 5, plane 91/88). (C) Slickenside lineations with strong grain comminution in left-lateral fault 170/63 (site 151). (D) Oblique normal fault plane (110/88) in dolerite dyke (site 167).

Guaxupé, was reactivated during the Late Permian as transpressional left-lateral, as the result of the collision of Patagonia Block and South America Platform (Rostirolla et al., 2000). Subsequently, a new, Late Cretaceous transtentional reactivation occurred, with right-lateral movement and smaller displacement. Ponta Grossa Arch is considered by some authors a basement NW–SE weakness reactivation (e.g., Ferreira, 1982a,b). Zalán et al. (1990) suggest that this direction was parallel to the maximum horizontal stress (SH_{max}) responsible for generating the Ribeira belt in southeastern Brazil during the Neoproterozoic Brasiliano orogeny, among other structures. The isopachs of the Ponta Grossa Formation (Devonian) and Itararé Group (Carboniferous–Permian), first presented by Northfleet et al. (1969), show the influence of the Ponta Grossa Arch over Paraná Basin sedimentation (Ferreira, 1982a).

3.5.2. D1 faults

D1 is represented by two sets of structures and probably related to two distinct directions and modulus (magnitude) of palaeostresses. The first group of structures includes N40–55W main extensional faults that allowed the intrusion of dolerite. After clockwise rotation and reduction of the SH_{max} module, local directional faults developed in outcrops of São Bento Group sandstones and dolerite. The faults into which dykes were emplaced underwent intense extensional movement, some presenting vertical displacement of more than 100 m, length greater than 50 km, and dykes up to 100 m wide. A NE–SW cross-section shows that N40–55W faults are subvertical and responsible for important layer tilting, usually with divergent dips from the axis of NW–SE fault zones (Fig. 18). Two sets of sigmoidal dykes are observed in aerial photographs, in which the geometric pattern and dip directions indicate a contemporaneous right-lateral movement during dolerite intrusion, corroborated by N30W en echelon splits (Fig. 19). It is important to note that kinematic indicators in mapped dykes are restricted to two fault zones in the central and northeast blocks. After magmatism, a set of N–S normal, N20W right-lateral, and N50E left-lateral conjugate faults originated by stress-field rotation and reduction in deformation magnitude. These faults show stronger shearing than D2 faults in basic rocks (cf. Fig. 17A and C) that generated cohesive breccia and crystalization of well-developed fibrous minerals within planes. In Pirambóia and Botucatu sandstones, the D1 record consists of a pair of conjugate strike-slip faults with reduced down-dip component. The N40W right-lateral faults (Fig. 13C) and N30E left-lateral faults represent the conjugate pair, which present en echelon fractures (R and R′ directions) and discrete grain comminution.

3.5.3. D2 faults

The D2 event generated the majority of faults observed in the field. In basic rocks, they usually present slickenside lineations and steps. In sandstones, the event manifests as deformation bands. In dolerite dykes, faults are different because of the intrusive body emplacement and the burial degree during faulting. In dykes, normal and normal-oblique faults predominate, whereas in Serra Geral extrusives, the faults are mostly strike-slip. Due to variation of the maximum horizontal stress (SH_{max}) between NE–SW and E–W directions, which correspond to σ_1 in extrusives and σ_2 in dykes, no contemporaneous set of structures could be characterized in basic rocks as typical of D2 (Fig. 20). Consequently, faults in igneous rocks show several directions compatible with the stress-field variation

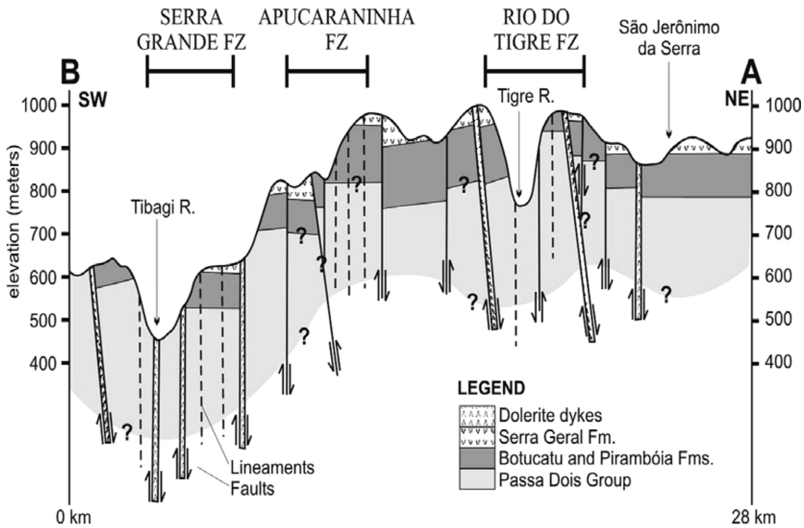

Fig. 18. Geologic NE–SW cross-section (see Fig. 5) showing strong structural compartmentation by NW–SE faults (Strugale et al., 2002).

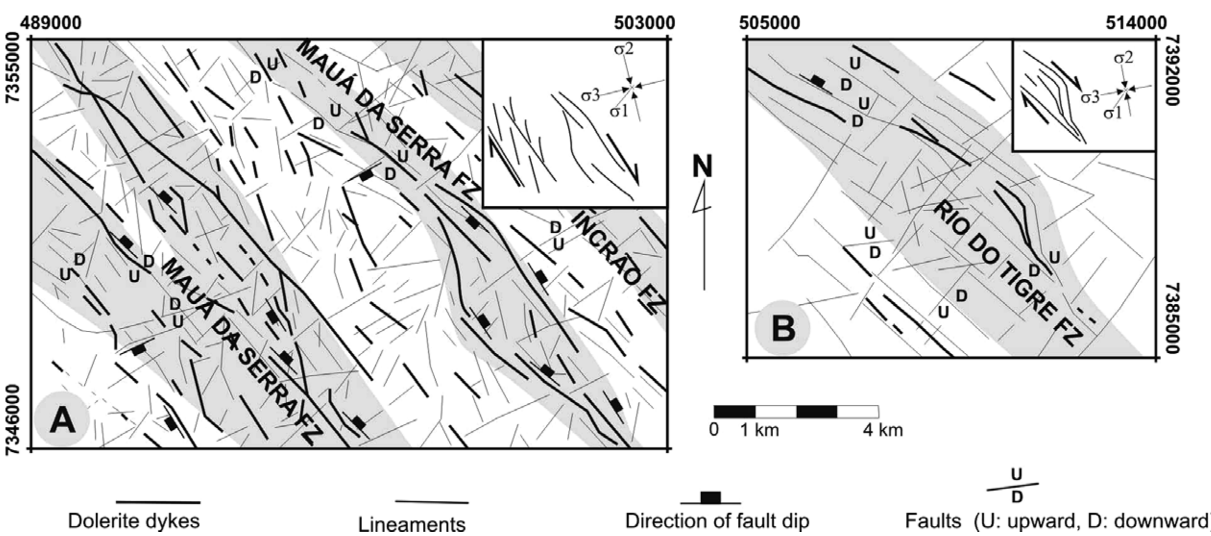

Fig. 19. Two examples of dykes showing sigmoidal geometry and right-lateral movement in accordance with local D1 stress. In both figures, the undulated geometry of the dykes follows fault traces.

amplitude. Another aspect of these rocks that relates to stress variation is their inherited discontinuities due to columnar joints and flow structures. Unlike in basalts, D2 is preserved in Pirambóia and Botucatu sandstones as well-defined pairs of conjugated faults, with N40–80W (mainly N65W) left-lateral synthetic faults and N40–60E right-lateral antithetic faults, mostly indicated by continuous deformation bands. Near the Apucaraninha Hydroelectric Power Plant (Fig. 5), conjugate Riedel directions are observed in a left-lateral fault zone. Regarding the strike-slip displacement, N66W/85E "Y," N85E/80NW "R," and N55W/85E "P" directions are observed (Fig. 15A and B). The conjugate joints R and R′ (Fig. 15C), oriented N66W/85NE (equivalent to strike-slip "Y" direction) and N65W/35SW, respectively, represent the down-dip component of fault zone. An example of fault reactivation by the D2 event is the D1 dyke sheared wall, whereas inner parts are preserved from deformation (Fig. 12). The SW wall contains the main fault and exhibits more intense deformation in the Rio do Rasto Formation (footwall block), with strong comminution, sigmoidal features (indicating down-dip faulting), and obliteration of sedimentary structures within a 5 m wide zone, which constitutes the D1 record. Normal antithetic faults in the hangingwall block and drag folding in pelitic beds also occur. A horizontal slickenside lineation (left-lateral) indicates D2 reactivation, which is much less intense than D1. Faults observed in the Marília Formation (Echaporã Member) of the Late Cretaceous Bauru Group show the following directions: NNE–SSW (right-lateral), ESE–WNW (left-lateral), ENE–WSW (normal left-lateral), and E–W (normal faults). The resulting stress directions modes are E–W related to σ_1, subvertical to σ_2, and N–S to σ_3. These directions are compatible with the average stress field of D2 event. In the Marília Formation, this event

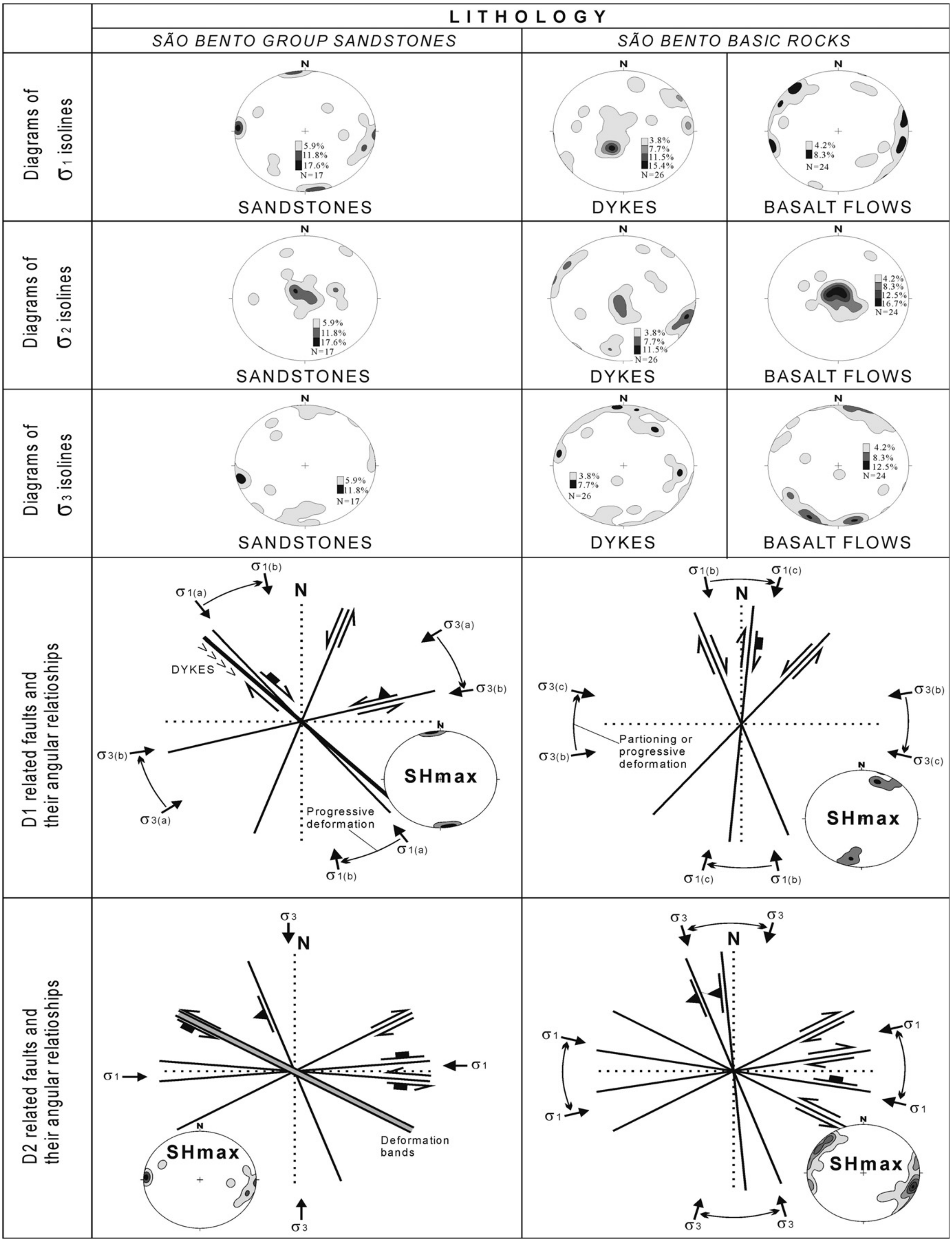

Fig. 20. Paleostresses and faults generated and/or reactivated during events D1 and D2 (diagrams of isolines: Schmidt Net, lower hemisphere). All faults measured during fieldwork.

shows a transtensional character, which can also be observed in the D2 phase of the studied area. In this unit, Riccomini (1995a) determined two tectonic events: one with an average σ_1 in E–W direction and another with average σ_1 in N–S direction.

3.6. Dynamic structural analysis

The dynamic analysis of faults based on linear kinematic indicators is represented in diagrams of maximum, mean, and minimum paleostress isolines (Fig. 20) for all faults, which identify stress concentration quadrants. These data determine the paleostress fields of the two deformation stages and their related fault generation and reactivation. Determination of paleostress using the Schmidt net was based on the Andersonian model, by which the first discontinuity is generated at 30° from σ_1, regardless of previous discontinuities. Thus, D1 is characterized by progressive deformation, and D2 reflects migration of SH_{max} around E–W and a deformation partition in underlying sandstones of the Pirambóia and Botucatu Formations.

Structural hierarchy and SH_{max} dispersion indicate that the most conspicuous D1 characteristic is its progressive deformation record, which results from an approximately 50° (N40W to N10E) clockwise rotation of the stress field, followed by a decrease in SH_{max} intensity. Evidence of such rotation and intensity decrease is that D1 facilitated intrusion of dykes and allowed brittle faulting, developed after dyke emplacement.

The early D1 deformation is mainly related to regional extensional faults with dolerite dyke intrusions at N40–55W and σ_1 at N40–445W ($\sigma_{1(a)}$ in Fig. 20). The dykes show local indicators of right-lateral movement during intrusion (Fig. 19), which could reflect the beginning of stress-field rotation, because they result from maximum and minimum stresses at N15–20W and N70–75E, respectively. The late D1 deformation ($\sigma_{1(b)}$ in Fig. 20) affected mainly sandstones of the São Bento Group, originating essentially brittle faults in the uppermost crustal levels after silicification by extrusion of the basalts of the Serra Geral Formation. Continuous SH_{max} rotation (transition from $\sigma_{1(b)}$ to $\sigma_{1(c)}$ in Fig. 20) is suggested by the N–S σ_1 orientation in sandstones and the N10–15E orientation in basic rocks. The difference in SH_{max} direction between sandstones and basic rocks indicates deformation partition due to both rheological differences and depth, or alternatively by continuous stress rotation. Thus, the absolute angular difference between $\sigma_{1(a)}$ and $\sigma_{1(c)}$ tensions can reach 50°.

Early D1 structures (dykes) are correlated with tectonic compartmentation controlled by N40–55W faulting (Fig. 18), during the Cretaceous geodynamic evolution of Ponta Grossa Arch (Figs. 6 and 21). The evolution of the arch at that time was affected by the thermal and structural uplift from SE toward NW, influenced by the Tristão da Cunha hot spot, which was also responsible for NE–SW crustal stretching, extrusive magmatism, and dyke intrusion. This extensional event has been reported by several authors studying South Atlantic Ocean spreading (Conceição et al., 1988; Chang and Kowsmann, 1991; Chang et al., 1992). During its evolution, the central block was more uplifted than the adjacent northeast and southwest ones, limited by the scissor-like regional faults, which were right-lateral at the NE border and, consequently, left-lateral in the SW segment of central block. Indicators of left-lateral movement were not observed in dykes of the SW portion of the study area, which suggests right-lateral movement as a main secondary or apparent strike-slip kinematic during stretching. According to Conceição et al. (1988), the most important activity of the Ponta Grossa Arch occurred between the end of the Permian and Cretaceous, as confirmed by isopachs of Upper Permian and Triassic + Jurassic units. Isopachs of Cretaceous basaltic extrusives are sectioned by the arch borders. Probably, the hotspot under the center of South Atlantic proto-Ocean resulted in the uplift of a thermal dome that made basement rocks more susceptible to ductile stretching. The differential oceanic spreading that resulted from this uplift began to the south of Walvis-São Paulo Ridge about 127 Ma and only at about 113 Ma to the north (Chang and Kowsmann, 1991). Its regional implications include the formation of the São Paulo Plateau on the SE Brazilian coast, which corresponds to a great mass of stretched continental crust intensely intruded by basic magmatic materials (Chang et al., 1992), and the formation of massive transitional evaporites in the Brazilian continental margin north of the plateau (Santos, Campos, and Espírito Santo basins). The arch partially absorbed the crustal stretching not completely compensated for in the oceanic area (São Paulo Plateau). Riccomini (1995b) reports that the generated stresses of the Ponta Grossa Arch acted at least until the Upper Cretaceous, with changes in σ_1 and σ_2 and the resulting first structural records of the Cananéia Alkaline Massif (K–Ar age ~82 My). A second event relates to an E–W oriented binary (similar to D2), with NW–SE extension and NE–SW compression, that deformed the massif. These tensions are compatible with the deformation of the tertiary continental rift of southeastern Brazil (Riccomini, 1989).

The main criteria for the distinction between D1 and D2 faults at outcrops of basic and sedimentary rocks are the more intense comminution on D1 fault planes (Fig. 17C), the timing of the two sets of structures, and the discontinuous, local character of postmagmatism D1 faults. Faults related to D2 are typically strike-slip with a secondary normal movement, where this type of deformation is better measured, as in the striated planes of the Serra Geral extrusives and dolerite dykes. Some strike-slip faults in sandstones show down-dip movement, as observed in the fault zone at the Apucaraninha Hydroelectric Power Plant (Fig. 15C). D2 also shows changes in the SH_{max} direction, with the mean value oriented to approximately N75W both for dykes and extrusives (Fig. 20). The timing of such changes cannot be determined. At least two distinct events could be responsible, but fault relationships at field scale

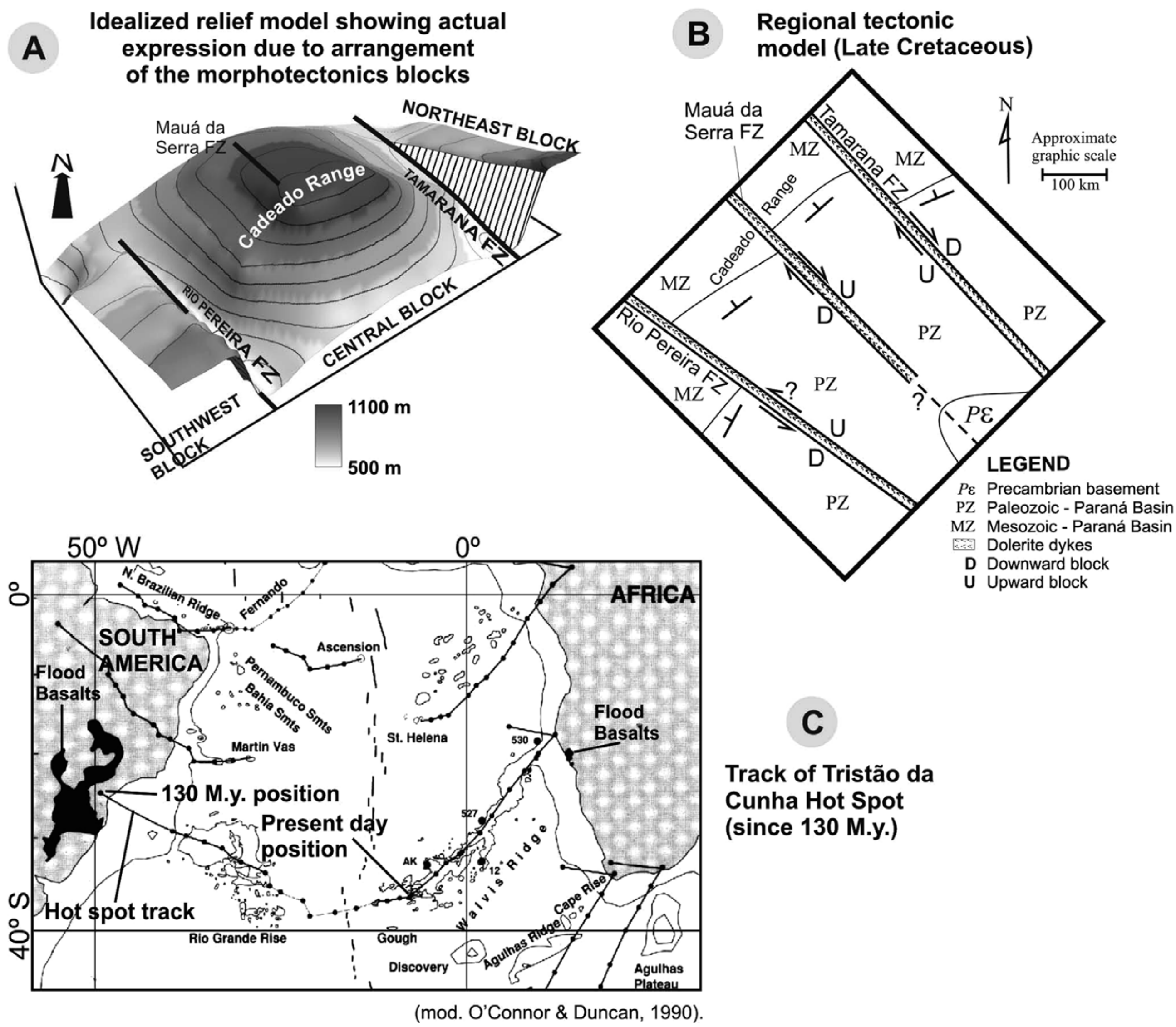

Fig. 21. Spatial distribution of Ponta Grossa Arch elements and a new Early Cretaceous structural compartmentation proposal, with the morphotectonic features (A) and main structures (B) related to Tristão da Cunha Hot Spot (C).

and the uniform frequency of isolines in the correspondent interval do not allow such determination (Figs. 9 and 20). The variation of SH_{max} between dykes and extrusives, which corresponds to stresses σ_2 and σ_1, respectively, can be explained by the contrast in confinement degree between these units at the time of deformation. The faults in dykes were measured in portions where they cut Paleozoic rocks (Passa Dois and Guatá groups), which were more confined than the extrusives during D2 event and thus increase lithostatic pressure by burial from extrusive basalts, which is added to the vertical D2 stress and becomes σ_1. Structures formed by reactivation of D1 faults during D2 appear in Fig. 12C. Brittle kinematic indicators show down-dip left-lateral movement on the main planes of these faults. Fault zones intruded by dykes (as in Fig. 12C), as well as comminution and sigmoidal features in the SW block, indicate extensional footwall deformation (Rio do Rasto Formation) during D1.

4. Discussion and conclusions

The axis of the Ponta Grossa Arch corresponds geographically to the Cadeado Range, which presents the highest altitudes (up to 1320 m) in central north Paraná. Altitudes decrease to the southwest and, with a smaller gradient, northeast. The important fault movements associated with the evolution of the arch led to intense segmentation of Pirambóia and Botucatu outcrop areas. A relief compartmentation is established by the altitudes at which these units outcrop. From the analysis of N40–55W photolineaments, fault zones can be identified, characterized by their higher density of dolerite dykes. Rio Pereira and Tamarana fault zones divide the study area into three morphotectonic compartments, each with particular relief altimetry variations and structural contour of Botucatu Formation (Fig. 21). The central block presents the highest altitudes and was more intensely deformed by

N40–55W structures, as recorded by higher photolineament density along that direction. Fault zones striking NW–SE are less conspicuous in NE and SW blocks.

The NW–SE fault zones present structural and topographic highs limited by rotational extensional scissor-like faults. The region most deformed by dyke intrusion coincides with a belt between the Rio Alonzo and São Jerônimo-Curiúva structural-magnetic alignments. The NW–SE fault zones' width and the geometry of internal fault traces are particular in their position relative to the axis of Ponta Grossa Arch. Other NW–SE fault zones are more planar and better marked on magnetic maps. The structural contour of the Botucatu Formation indicates strong segmentation caused by NW–SE fault zones, represented by morphotectonic blocks, which suggest development of a thermal anomaly, probably induced by the Tristão da Cunha Hot Spot, positioned in eastern Paraná in the Early Cretaceous O'Connor and Duncan (1990).

The morphotectonic compartmentation of the study area by NW–SE rotational faults led to a central block higher and more displaced to northwest than its adjacent ones (Fig. 21). The great number of dykes present, mainly concentrated in the central block, justifies the space generation brought about by the thermal anomaly. On the basis of magnetic and gravimetric models of a segment of the Guapiara alignment, Ferreira et al. (1981, 1989) estimated a crustal stretching of 14%, a maximum mantle ascent of 5 km, and a horizontal minimum extension of 18%, because brittle fracturing was preceded by a ductile, non-estimated extension. In the central portion of the arch, delimited by the Rio Alonzo and São Jerônimo-Curiúva lineaments, Portela Filho (2002) calculated a minimum crustal extension of 13%, based on dyke-induced and remanent magnetic anomaly models from residual magnetic data (Fig. 9). The presence of basement weakness zones (Ferreira, 1982a,b; Zalán et al., 1990) favored the highest dyke concentration between Rio the Alonzo and São Jerônimo-Curiúva structural-magnetic alignments. These parameters are compatible with the results of the structural analysis of the first deformation phase defined herein and the Mesozoic and Cenozoic tectonic interpretation of Ponta Grossa Arch reported by Riccomini (1995a,b).

Two tectonic events are distinguished, D1 and D2. Each event affected the units at different burial depths. D1 relates to brittle faults, whereas D2 took place at a time when sandstones were under the load represented by Serra Geral Formation.

D1 was responsible for the most prominent regional structures in the study area and controlled the intrusion of the dyke swarm. The stratigraphic data suggest that uplift was preceded by erosion of the Triassic Pirambóia Formation in the axis of the arch, followed by almost flat Botucatu aeolian sandstones (Late Jurassic) and Serra Geral (138–127 My) flows. The aeolian sedimentation and fissural volcanism probably occurred after uplift and extensive erosion. D1 structures are products of progressive deformation caused by a 20–30° clockwise rotation of SH_{max} stress field, which establishes time and scale hierarchy. At the beginning, D1 stresses were basically extensional and controlled regional uplift and dyke intrusion at a regional scale. Related features indicate a secondary right-lateral movement during the intrusion of some dyke swarms. The latter record is usually observed in sandstones as conjugated pairs of non-continuous strike-slip faults (N40W right-lateral synthetic, N30E antithetic) that, together with other correlated faults in dykes, are compatible with σ_1 along N10W. In absolute terms, the clockwise rotation of SH_{max} during D1 reached estimated values of approximately 50° (30° average), based on faults in São Bento Group rocks. The most likely hypothesis for this absolute rotation is that faulting was kinematically induced by a local stress field. Block movement also generated second-order structures by partitioning of deformation.

D2 presents the most systematic structural record observed at outcrops. A Late Cretaceous–Tertiary time position is defined for this event. The D2 main characteristic is variation in paleostress orientation, related to the geometry and spatial distribution of igneous rock bodies (extrusives and dykes) and the degree of confinement at the time of deformation. Unlike in D1, ages or stages of variation of D2 tension field do not correspond to progressive deformation but rather are defined as a continuous movement of SH_{max} between N75E and N40W. Unlike basic rocks, D1 faults in sandstones were generated by SH_{max} around E–W. In general, D2 behavior is transtensional and characterized by: (1) strike-slip and extensional faults in Serra Geral extrusives, where SH_{max} corresponds to σ_1; and (2) predominantly oblique extensional faults in dolerite dykes, with SH_{max} corresponding to σ_2. Another particular aspect of D2 is the migration of SH_{max} between N75E and N40W (Fig. 20), though their relative ages are unknown. D2 is recorded in sandstones as a conjugated pair of continuous deformation bands; the more developed synthetic (left-lateral) direction is N45–60W compared with the antithetic, N60E right-lateral. In these structures, directions of σ_1 consistently average N85W. D2 deformation is concentrated in dyke walls by their reactivation (Fig. 10) and, perhaps as a result, σ_1 directions in sandstones are less dispersed than in basic rocks. Deformation bands in D2 faults result from higher lithostatic and fluid pressure conditions due to the overlying Serra Geral basalts, which caused deformation of unconsolidated or semiconsolidated materials that show plastic features (Fig. 15B). The main direction of deformation bands is N50W. Many authors have discussed the D2 stress field, with σ_1 oriented E–W during Cenozoic, such as at the continental rift of southeastern Brazil (Riccomini, 1989, 1995a,b). Seismologic data (Assumpção, 1992) and oil well breakouts (Lima and Nascimento, 1994; Riccomini, 1995a) also corroborate Quaternary E–W compression continuing to act up to the present day.

Acknowledgements

The authors thank CNPq (Grant 463002/008), FINEP, and PETROBRAS for financial support. We are grateful to Bárbara Trzaskos-Lipski and Isabella F.R. Figueira for revising the first draft and to Dr. Rodolfo José Angulo (Departamento de Geologia – UFPR) for having revised the final text. Michael Strugale thanks CAPES for a master's degree scholarship, and Sidnei Pires Rostirolla appreciates financial support from CNPq. The authors thank the reviewers for their profitable suggestions to improve the manuscript.

References

Assumpção, M., 1992. The regional interplate stress field in South America. J. Geophys. Res. 97, 11.889–11.903.

Bastani, M., Pedersen, L.B., 2001. Automatic interpretation of magnetic dyke parameters using the analytical signal technique. Geophysics 66, 551–561.

Billings, M.P., 1972. Structural Geology, third ed. Prentice-Hall, New Jersey, 606p.

Briggs, I.C., 1974. Machine contouring using minimum-curvature. Geophysics 39, 39–48.

Chang, H.K., Kowsmann, R.O., 1991. Significado dos diques do Arco de Ponta Grossa na abertura diferencial do Atlântico Sul. III Simpósio Nacional de Estudos Tectônicos, pp. 77–78.

Chang, H.K., Kowsmann, R.O., Figueiredo, A.M.F., Bender, A.A., 1992. Tectonics and stratigraphy of the East Brazil Rift system: an overview. Tectonophysics 213, 97–138.

Conceição, J.C., Zalán, P.V., Wolff, S., 1988. Mecanismo, evolução e cronologia do rift Sul-atlântico. Bol. Téc. Petrobrás 2 (2), 255–265.

Davis, G.H., Bump, A.P., García, P.E., Ahlgren, S.G., 1999. Conjugate Riedel deformation band shear zones. J. Struct. Geol. 22, 169–190.

Ferreira, F.J.F., 1982a. Integração de dados aeromagnéticos e geológicos: configuração e evolução tectônica do Arco de Ponta Grossa. MSc Thesis. Inst. de Geociências, Universidade de São Paulo, São Paulo, Brazil, 170p.

Ferreira, F.J.F., 1982b. Alinhamentos Estruturais – Magnéticos da Região Centro-oriental da Bacia do Paraná e seu significado tectônico – Reavaliação da Potencialidade e Prospectividade em Hidrocarbonetos. Consórcio CESP-IPT, pp. 144–166.

Ferreira, F.J.F., Monma, R., Campanha, G.A.C., Galli, V.L., 1989. An estimate of the degree of crustal extension and thinning associated with the Guapiara Lineament based on aeromagnetic modelling. Bol. IG-USP Série Científica 20, 70–96.

Ferreira, F.J.F., Moraes, R.A.V., Ferrari, M.P., Vianna, R.B., 1981. Contribuição ao estudo do Alinhamento Estrutural de Guapiara. III Simpósio Regional Geologia. Curitiba. V1, pp. 226–240.

Ferreira, F.J.F, Portela Filho, C.V., 2001. Mapa magnético do estado do Paraná (parcial). Laboratório de Pesquisas em Geofísica Aplicada (LPGA), Departamento de Geologia, Universidade Federal do Paraná – UFPR.

Geosoft, 2001. Microlevelling using bi-directional gridding. Geosoft Technical Note, 2p.

Hsu, S.-K., Coppens, D., Shyu, C.-T., 1998. Depth to magnetic source using the generalized analytical signal. Geophysics 63, 1947–1957.

Hsu, S.K., Sibuet, J.-C., Shyu, C.-T., 1996. High-resolution detection of geologic boundaries from potential field anomalies: an enhanced analytic signal. Geophysics 61, 373–386.

Lima, C.C., Nascimento, E., 1994. Stress orientations in Brazilian sedimentary basins from breakout analysis: implications for force models in the South Amrican plate. Geophys. J. Int. 130 (1), 112–124.

Magnavita, L.P., 2000. Deformation mechanics in porous sandstones: implications for development of fault seal and migration paths in the Recôncavo Basin, Brazil. In: Melo, M.R., Katz, B.J. (Eds.) Petroleum Systems of South Atlantic Margins, vol. 73. AAPG Memoir, pp. 195–212.

Milani, E.J., França, A.B., Schneider, R.L., 1994. Bacia do Paraná. Bol. de Geoc. da Petrobrás 8 (1), 69–82.

Milani, E.J., Ramos, V.A., 1998. Orogenias Paleozóicas no domínio sul-ocidental do Gondwana e os ciclos de subsidência da Bacia do Paraná. Rev. Bras. de Geoc. 24 (4), 473–484.

Minty, B.R.S., 1991. Simple micro-levelling for aeromagnetical data. Exploration Geophys. 22, 591–592.

Nabighian, M.N., 1972. The analytic signal of two-dimensional magnetic bodies with poligonal cross-section: its properties and use for automated anomaly interpretation. Geophysics 37, 507–517.

Nabighian, M.N., 1974. Additional comments on the analytic signal of two-dimensional magnetic bodies with polygonal cross-section. Geophysics 39, 85–92.

Northfleet, A.A., Medeiros, R.A., Muhlmann, H., 1969. Reavaliação dos dados geológicos da Bacia do Paraná. Bol. Téc. da Petrobrás 13 (3), 291–346.

O'Connor, J.M., Duncan, R.A., 1990. Evolution of the Walvis Ridge-Rio Grande Rise Hot Spot system: Implications for African and South America plate motions over plumes. J. Geophys. Res. 95 (B11), 475–512.

Portela Filho, C.V. 2002. Condicionamento estrutural-magnético do Sistema Aqüífero Serra Geral na região central do Arco de Ponta Grossa (Bacia do Paraná) e sua conectividade com o Sistema Aqüífero Guarani. MSc Thesis. Curitiba, Universidade Federal do Paraná, 122p.

Renne, P.R., Ernesto, M., Pacca, I.G., Coe, R.S., Glen, J.M., Prévot, M., Perrin, M., 1992. The age of Paraná flood volcanism, rifting of Gondwanaland, and the Jurassic–Cretaceous boundary. Science 258, 957–959.

Riccomini, C, 1989. O Rift Continental do sudeste do Brasil. Ph.D. Thesis, Inst. Geociências, Universidade de São Paulo, São Paulo, Brazil, 256p.

Riccomini, C, 1995a. Tectonismo Gerador e Deformador dos Depósitos Sedimentares Pós-Gondvânicos da Porção Centro-oriental do Estado de São Paulo e Áreas Vizinhas. Tese de Livre-Docência, Inst. de Geociências, Universidade de São Paulo, São Paulo, Brazil, 100p (restricted circulation).

Riccomini, C., 1995b. Padrão de fraturamentos do Maciço Alcalino de Cananéia, Estado de São Paulo: relações com a tectônica mesozóica-cenozóica do sudeste do Brasil. Rev. Bras. de Geoc. 25 (2), 79–84.

Rocha-Campos, A.C., Cordani, U.G., Kawashita, K., Sonoki, H.M., Sonoki, I.K., 1988. Age of Paraná Flood volcanism. In: Piccirillo, E.M., Melphi, A. (Eds.), The Mesozoic Flood Basalts of the Paraná Basin: Petrogenetic and Geophysical Aspects. Instituto Astronômico e Geofísico – USP, pp. 25–41.

Rostirolla, S.P., Assine, M.L., Fernandes, L.A., Artur, P.C., 2000. Reativação de Paleolineamentos durante a Evolução da Bacia do Paraná – O Exemplo do Alto Estrutural de Quatiguá. Rev. Bras. de Geoc. 30 (4), 639–648.

Rostirolla, S.P., Mancini, F., Rigoti, A., Kraft, R.P., 2003. Structural styles of intracratonic reativation of the Perimbó Fault Zone, Paraná Basin, Brazil. J. South Am. Earth Sci. 16, 287–300.

Soares, P.C., 1975. Divisão Estratigráfica do Mesozóico no Estado de São Paulo. Rev. Bras. de Geoc. 5 (4), 229–251.

Soares, P.C., 1992. Tectônica sin-sedimentar cíclica na Bacia do Paraná: controles. Departamento de Geologia, Universidade Federal do Paraná, Curitiba, Full Professor Thesis, 148p.

Soares, P.C., Landim, P.M.B., Fúlfaro, V.J., 1978. Tectonic cycles and sedimentary sequences in the Brazilian intracratonic basins. GSA Bull. 89, 181–191.

Stewart, K., Turner, S., Kelley, S., Hawkesworth, C., Kirstein, L., Mantovani, M., 1996. 3-D, ^{40}Ar–^{39}Ar geochronology in the Paraná continental flood basalt province. Earth Planet. Sci. Lett. 143, 95–109.

Strugale, M. 2002. Arcabouço e evolução estrutural do Arco de Ponta Grossa no Grupo São Bento (Mesozóico): Implicações na hidrodinâmica do Sistema Aqüífero Guarani e na migração de hidrocarbonetos na Bacia do Paraná. MSc Thesis, Departamento de Geologia, Universidade Federal do Paraná – UFPR, 138 p.

Strugale, M., Rostirolla, S.P., Rosa Filho, E.F., Mancini, F., Hindi, E.C., Ferreira, F.J.F., Freitas, R.C. 2002 Geologia estrutural do Arco de Ponta Grossa no centro-norte do Estado do Paraná (Brasil): implicações na hidrodinâmica do Sistema Aqüífero Guarani (CD-ROM). XII Congresso Brasileiro de Águas Subterrâneas, Florianópolis, Brazil.

Strugale, M., Rostirolla, S.P., Mancini, F., Portela Filho, C.V., 2004. Compartimentação Estrutural das formações Pirambóia e Botucatu na região de São Jerônimo da Serra – Estado do Paraná. Rev. Bras. de Geoc. 34 (3), 303–316.

Turner, S., Regelous, M., Kelley, S., Hawkesworth, C., Mantovani, M., 1994. Magmatism and continental break-up in the South Atlantic: high precision $^{40}Ar/^{39}Ar$ geochronology. Earth Planet. Sci. Lett. 121, 333–348.

Ussami, N., Kolisnik, A., Raposo, M.I.B., Ferreira, F.J.F., Molina, E.C., Ernesto, M., 1991. Detectabilidade magnética dos diques do Arco de Ponta Grossa: um estudo integrado de magnetometria terrestre/aérea e magnetismo de rocha. Rev. Bras. Geoc. 21 (4), 317–327.

Vieira, A.J., 1973. Geologia do Centro e Nordeste do Paraná e Centro-sul de São Paulo. XXVIII Congresso Brasileiro de Geologia V. 3, pp. 259–277.

Zalán, P.V., Wolff, S., Astolfi, M.A.M., Vieira, I.S., Conceição, J.C.J., Appi, V.T., Neto, E.V.S., Cerqueira, J.R., Marques, A., 1990. The Paraná Basin, Brazil. AAPG Memoir 51, 681–708.